SANDIA REPORT
SAND2010-5071
Unlimited Release
Printed July 2010

Network Design Optimization of Fuel Cell Systems and Distributed Energy Devices

Whitney G. Colella

Prepared by
Sandia National Laboratories
Albuquerque, New Mexico 87185 and Livermore, California 94550

Sandia National Laboratories is a multi-program laboratory managed and operated by Sandia Corporation, a wholly owned subsidiary of Lockheed Martin Corporation, for the U.S. Department of Energy's National Nuclear Security Administration under contract DE-AC04-94AL85000.

Issued by Sandia National Laboratories, operated for the United States Department of Energy by Sandia Corporation.

Available to DOE and DOE contractors from
U.S. Department of Energy
Office of Scientific and Technical Information
P.O. Box 62
Oak Ridge, TN 37831

Telephone: (865) 576-8401
Facsimile: (865) 576-5728
E-Mail: reports@adonis.osti.gov
Online ordering: http://www.osti.gov/bridge

Available to the public from
U.S. Department of Commerce
National Technical Information Service
5285 Port Royal Rd.
Springfield, VA 22161

Telephone: (800) 553-6847
Facsimile: (703) 605-6900
E-Mail: orders@ntis.fedworld.gov
Online order: http://www.ntis.gov/help/ordermethods.asp?loc=7-4-0#online

SAND2010-5071
Unlimited Release
Printed July 2010

Network Design Optimization of Fuel Cell Systems and Distributed Energy Devices

Whitney G. Colella
Energy Resources and Systems Analysis Division
Sandia National Laboratories
P.O. Box 5800
Albuquerque, New Mexico 87185-1108

Abstract

This research explores the thermodynamics, economics, and environmental impacts of innovative, stationary, polygenerative fuel cell systems (FCSs). Each main report section is split into four subsections. The first subsection, "Potential Greenhouse Gas (GHG) Impact of Stationary FCSs," quantifies the degree to which GHG emissions can be reduced at a U.S. regional level with the implementation of different FCS designs. The second subsection, "Optimizing the Design of Combined Heat and Power (CHP) FCSs," discusses energy network optimization models that evaluate novel strategies for operating CHP FCSs so as to minimize (1) electricity and heating costs for building owners and (2) emissions of the primary GHG — carbon dioxide (CO_2). The third subsection, "Optimizing the Design of Combined Cooling, Heating, and Electric Power (CCHP) FCSs," is similar to the second subsection but is expanded to include capturing FCS heat with absorptive cooling cycles to produce cooling energy. The fourth subsection, "Thermodynamic and Chemical Engineering Models of CCHP FCSs," discusses the physics and thermodynamic limits of CCHP FCSs.

Acknowledgments

This research was supported in part by an appointment to the Sandia National Laboratories Truman Fellowship in National Security Science and Engineering, sponsored by Sandia Corporation (a wholly owned subsidiary of Lockheed Martin Corporation) as operator of Sandia National Laboratories (SNL) under its U.S. Department of Energy Contract No. DE-AC04-94AL85000. The authors wish to thank the Laboratory Directed Research and Development office at SNL for spurring innovation through the Truman postdoctoral fellowship. Sincere gratitude goes to Henry Westrich and Charles Barbour for their help supporting this research.

The author wishes to thank Professor Stephen H. Schneider of Stanford University; Professor Daniel M. Kammen of the University of California at Berkeley; Aerel Rankin of the University of New Mexico; Professor Jack Brouwer, Pere Margalef, and Sarah Kelly Martz of the University of California at Irvine; and Matt Abbott of Texas A&M University for research contributions to this work. For reviewing this work and providing guidance at SNL, the author wishes to thank (in alphabetical order, by last name) Abbas Akhil, Mike Hightower, and Ron Stoltz. For facilitating the use of SNL's Exergy Lab, many thanks are owed to Jeff Carlson, Juan Torres, and David Wilson. For running models on SNL's parallel computing cluster in the Advanced Information Systems Lab (AISL), the author sincerely thanks Marvin Cook, Steven Goldsmith, and Shannon Spires. For leadership in energy systems at SNL, the author wishes to thank Terry Michalske, Rush Robinett, Les Shepard, Ellen Stechel, Margie Tatro, and Juan Torres.

In addition, the author wishes to express gratitude to the following individuals (in alphabetical order, by affiliation):

- Colorado School of Mines: Robert Braun, Nigel Sammes, and Ryan Timme
- Constructive Choices, Inc.: Jean Strosinski
- FuelCell Energy, Inc.: Joe Heinzmann, Fred Jahnke, Tony Leo, Chris Pais, Pinakin Patel, and Trevor Rodd
- Gas Technology Institute: Ron Stanis
- Golden State Energy, Inc.: Thomas A. Damberger
- Lawrence Berkeley National Laboratory (LBNL): Jonathan Koomey
- Penn State University: Michael Alley, Michael Hickner, and Katherine Nicol
- Sandia National Laboratories: Abbas Akhil, Michael Baca, Rita Baca, Joey Baiardo, Lenore Boulton, John Boyes, Patrick Brady, Jennifer Byers, Jeff Carlson, Ken Chen, Marvin Cook, Tom Corbet, Louise Criscenti, Annie Day, Patricia Falcone, Peter Feibelman, Gina Fresquez, Cy Fujimoto, Marie Garcia, Roberta Gonzales, Stephen Goldsmith, Susanna Gordon, Don Hardesty, Jacquelynne Hernandez, Mike Hightower, Mark Ivey, Lance Jensen, Gio Kao, Mark Linne, Annie McIntyre, Terry Michalske, Marcina Moreno, Yolanda Moreno, Jeff Nelson, Nancy Nicolary, Rush Robinett, Paul Rockett, Ewa Ronnebro, Robert Scheffer, John Shelnutt, Les Shepard, Kayla Smith, Yujiang Song, Shannon Spires, Jason Stamp, Ellen Stechel, Jennifer Stinebaugh, Ron Stoltz, Margie Tatro, Laurel Taylor, Joe Tillerson, Juan Torres, Jeff Tsao, Albert Valdez, David Wilson, Wendy Wolfson, Bernie Zak; and Divisions 6300, 8300, and 8700

- Stanford University: Sarah Jo Chadwick, Scott Gould, Aditya Jhunjhunwala, Susan Kulakowski, Patricia Mastrandrea, Dean Murray, Melahn Parker, Stephen H. Schneider, Nigel Teo, Matthew Tilghman, and the Stanford Utilities Division
- Sun Microsystems: Kenneth Russell
- Texas A&M University: Matthew Abbott
- United Technologies, Inc.: Ed Baker, David D. Brengel, John Ferro, Jack Gatzuras, Manish Khandelwal, Thomas Madden, Kent McCord, Mike L. Perry, Ram Ramaswamy, Margaret M. Steinbugler, Eric R. Strayer, and Bob Tierney
- University of California at Berkeley: Daniel M. Kammen
- University of California at Irvine: Jack Brouwer, Pere Margalef, and Sarah Kelly Martz
- University of New Mexico: Andrea Mammoli, David Menicucci, and Aerel Rankin
- U.S. Department of Energy's (DOE's) Energy Information Administration (EIA): James K. Joosten, Tom Leckey, Perry Lindstrom, Kevin Lillis, Channele Wirman, and Orhan Yildiz
- U.S. Department of Energy's (DOE's) Energy Efficiency and Renewable Energy (EERE) Fuel Cells and Transportation Programs: Christy Cooper, Peter Devlin, John Garback, Nancy Garland, Fred Joseck, Jason Marcinkoski, Dimitrios Papageorgopoulos, Carole Read, Drew Ronneberg, and Nguyen D. Tien

Many thanks are also owed to the various reviewers for their comments on the report.

Contents

Figures

Tables

Executive Summary

Potential Greenhouse Gas (GHG) Impact of Stationary Fuel Cell Systems (FCSs)
The first subsection describes the role that stationary FCSs and different fuel cell types — including solid oxide fuel cell (SOFC), molten carbonate fuel cell (MCFC), proton exchange membrane fuel cell (PEMFC), and phosphoric acid fuel cell (PAFC) — can play in meeting California's newly legislated carbon dioxide (CO_2) emission reduction targets. As the seventh largest economy world-wide and the twelfth largest greenhouse gas (GHG) emitter, California emits 22% of its emissions in the electric power sector. To comply with new legislation (specifically, the California Global Warming Solutions Act of 2006, also known as Assembly Bill 32 [AB32]) [1], the state must reduce its GHG emissions by 2010 to the 2000 levels, and by 2020 to the 1990 levels. Under the California Governor's Executive Order S-3-05 [2], by 2050, the state must reduce its emissions to 80% lower than its 1990 levels. Based on an analysis of complete historical CO_2 emission data, this research quantifies the expected reductions in CO_2 emissions with the introduction of stationary distributed FCSs of different types. The results have been generalized so that they are relevant to all world regions.

Optimizing the Design of Combined Heat and Power (CHP) FCSs
The second subsection describes energy network optimization models developed to identify new strategies for designing, installing, and controlling stationary cogenerative FCSs to minimize (1) electricity and heating costs for building owners and (2) emissions of the primary GHG — CO_2. A main goal of this work is to employ relatively inexpensive computer simulation studies to identify more financially and environmentally effective approaches for installing FCSs. Models quantify the impact of different choices made by power generation operators, FCS manufacturers, building owners, and governments with respect to two primary goals — energy cost savings for building owners and CO_2 emission reductions. These types of energy system models are crucial for identifying cost and CO_2 optima for particular installations because optimal strategies can change with varying engineering performance, market conditions, and environmental needs. Optimal strategies can change with variations in FCS performance, the characteristics of building demand for electricity and heat, and many other factors. Models evaluate both ~~"b~~usiness-as-usual" and novel FCS operating strategies. For the scenarios examined here, relative to a base case of no FCSs installed, models indicate that novel strategies could reduce building energy costs by 25% and CO_2 emissions by 80%. This report initially discusses the motivation and key assumptions behind model development. Subsequently, this report discusses model run results for the case study of a California town and makes recommendations for further FCS installments applicable to many regions.

Model results show that the most optimal strategies for cost and CO_2 savings differ, but both invoke novel approaches. The strategy with the highest cost savings combines cogeneration, networking, variable heat-to-power (VHP) ratio, no load following for the primary control at maximum electrical output, and subsequent heat load following for the secondary control. Results assume a base case with no FCSs installed and most power and heat provided by a cogenerative combined cycle gas turbine and any additional electricity supplied by the average mix of power plants in California. Relative to the base case, this strategy results in an approximate 25% cost reduction. Similarly, the strategy with the highest CO_2 emission savings combines cogeneration, networking, VHP, heat load following for the primary control, and

subsequent no load following for the secondary control. Relative to the base case, this strategy results in CO_2 savings of 80%. Energy costs and CO_2 emissions can be reduced significantly by switching from certain ―business-as-usual" approaches to novel ones; specifically from (1) stand-alone to networked, and then from (2) fixed heat-to-power ratio to variable. Switching from a ―business-as-usual" approach to a novel one can improve energy cost savings more than an approach of retaining a ―business-as-usual" approach while increasing the carbon tax from $0 to $100/metric tonnes of CO_2. A carbon tax can provide more cost savings when combined with novel approaches rather than with ―business-as-usual" ones.

Optimizing the Design of Combined Cooling, Heating, and Electric Power (CCHP) FCSs

The third subsection describes innovative design, installation, and control strategies for generating CCHP with FCSs. The addition of an absorptive cooling cycle (ACC) allows FCS unrecovered heat to be used for air-conditioning. Low-temperature unrecovered heat (80–160 °C) can be used to drive absorption chillers to create a chilled water stream to cool building spaces. Compared with separate devices that individually generate electricity, heat, and cooling power, such CCHP FCSs can reduce feedstock fuel consumption by about 50%. Economic and environmental models were developed that optimize CCHP FCS installed capacity to minimize global CO_2 emissions or global energy costs from generating cooling power, heat, and electricity. Our models evaluate innovative engineering design, installation, and control strategies not commonly pursued by industry, and identify strategies most beneficial for CO_2 emission or cost reductions. Models minimize costs for building owners consuming cooling power, electricity, and heat by changing the installed capacity of FCSs and FCS operating strategy. Models optimize for a particular location, climatic region, building load curve set, FCS type, and competitive environment. Innovative approaches evaluated include networking for cooling power, heat, and electricity; using a VHP; using a tunable output of total cooling to recoverable heat; and load following cooling, heat, or electricity demands. Example results are shown for a California town based on realistic input assumptions and conclusions are drawn that are applicable to a broad cross-section of world regions.

Thermodynamic and Chemical Engineering Models of CCHP FCSs

The fourth subsection evaluates the thermodynamics and chemical engineering design of high-temperature FCSs coupled with ACCs. Double-effect lithium bromide (LiBr) ACC models are developed and deployed to analyze the effects of the fuel cell exhaust gas temperature, fuel cell stack current density, fuel cell stack fuel utilization factor (U_f), and other variables on CCHP FCS performance. FCS submodels describe SOFC electrical efficiency and power output as a function of current density, operating temperature, pressure, and inlet fuel and oxidant characteristics. LiBr ACC models describe the energy and mass balance around various streams in the device, and consider second law limitations as well. LiBr ACC models are verified against industrial data for coefficient of performance (COP) as a function of temperature, and cooling power output as a function of inlet flow rate. Models reveal the expected performance for thermally integrated CCHP FCSs. This performance includes efficiency (electrical, heat, and cooling) and cooling power output as a function of fuel flow rate, operating temperature, current density, and a variety of other operating conditions. The combined overall efficiency of CCHP FCS (including electrical, heat, and cooling efficiency) is expected to be greater than that of CHP FCSs when the LiBr ACC COP is greater than one.

Nomenclature

ACC	Absorptive Cooling Cycle
BTU	British Thermal Unit
C	Cooling Load Following
$\mathbf{C_{p,n}}$	Constant-pressure heat capacity of stream n entering SHX
CCGT	Combined Cycle Gas Turbine
CCHP	Combined Cooling, Heating, and Electric Power
CEC	California Energy Commission
CHP	Combined Heat and Power
CO_2	Carbon Dioxide
COP	Coefficient of Performance
CR	Circulation Ratio, ratio of mass flow of concentrated solution to refrigerant
DOE	Department of Energy
E	Electric Load Following
EIA	Energy Information Agency
EN	Electrical Minimum
EX	Electrical Maximum
$\boldsymbol{\epsilon_{elec}}$	Overall net electrical efficiency of a CCHP FCS
$\boldsymbol{\epsilon_{heat}}$	Overall heat recovery efficiency of a CCHP FCS
$\boldsymbol{\epsilon_{cooling}}$	Overall cooling power efficiency of a CCHP FCS
F or FHP	Fixed Heat-to-Power Ratio
F	Faraday constant (96,486 C/mol)
FCE	FuelCell Energy, Inc.
FCS	Fuel Cell System
GHG	Greenhouse Gases
$\boldsymbol{\Delta G_{rxn}(T)}$	Gibbs free energy of reaction
$\mathbf{h_n}$	Enthalpy per unit mass (kJ/kg) of stream n
$\boldsymbol{\Delta H_{rxn}}$	Change in enthalpy for a reaction
$\boldsymbol{\Delta H_{rxn,\,fc}}$	Heat of reaction for the oxidation of H_2 and/or CO within the fuel cell stack (kJ), according to the reactions $H_2 + ½\ O_2 \rightarrow H_2O$ and/or $CO + ½\ O_2 \rightarrow CO_2$
H_2	Hydrogen
HHV	Higher heating value

H or HLF	Heat Load Following
HN	Heat Minimum
HX	Heat Maximum
i	Current generated from the fuel stack (A).
j	Current density (A/m^2)
$\mathbf{j_{o,*}}$	Exchange current density at cathode and at anode (A/m^2)
$\mathbf{j_L}$	Limiting current density (A/m^2)
K	Chemical reaction equilibrium constant
kJ	Kilojoules
kWe	Kilowatt of Electric Power
LiBr	Lithium Bromide
$\mathbf{\dot{m}_n}$	Mass Flow Rate of Stream n
MCFC	Molten Carbonate Fuel Cell
MMT	Million Metric Tonnes
MT	Metric Tonne
MWe	Mega-Watt of Electric Power
N	Networked
NLF	No-Load Following
$\mathbf{n_e}$	Number of electrons transferred during the oxidation process
$\mathbf{p_i}$	Partial pressure of the i^{th} component. i = *ambient*, O_2, H_2O, and H_2.
$\mathbf{P_{grosselec}}$	Gross electrical power output of the fuel cell stack
$\mathbf{P_{parasitic}}$	Electrical parasitic loads associated with compression and pumping
PAFC	Phosphoric Acid Fuel Cell
PEMFC	Proton Exchange Membrane Fuel Cell
PM	Particulate Matter
$\mathbf{Q_{FC}}$	Total heat released by the fuel cell stack and sub-system, (kJ)
$\mathbf{Q_y}$	Heat flux (kW) to/from component y
$\mathbf{R_k}$	Ohmic resistance of k^{th} material, *k = anode, cathode, interconnect, and electrolyte*
$\mathbf{R_u}$	Universal Gas Constant, (0.08205 L atm/mol/K)
S	Stand-Alone
SHX	Solution Heat Exchanger
SOFC	Solid Oxide Fuel Cell
SNL	Sandia National Laboratories

STP	Standard Temperature and Pressure
T	Tunable Heat-to-Cooling Ratio
$\mathbf{T_{out}}$	Temperature
V or VHP	Variable Heat-to-Power Ratio
$\mathbf{V^{ideal}}$	Ideal Voltage
$\mathbf{W_{elec}}$	Electric work output of the fuel cell stack, (kJ)
$\mathbf{W_{elec}^{ideal}}$	Reversible, maximum electric work
$\mathbf{X_n}$	Mole fraction of Lithium Bromide (LiBr) in stream n
$\boldsymbol{\psi_{SHX}}$	Solution heat exchanger effectiveness
$\boldsymbol{\eta_{act}}$	Polarization or voltage loss due to activation of chemical reactions
$\boldsymbol{\eta_{conc}}$	Polarization or voltage loss due to concentration gradient
$\boldsymbol{\eta_{ohm}}$	Polarization or voltage loss due to internal ohmic resistance

1. Introduction

1.1. Potential Greenhouse Gas (GHG) Impact of Stationary Fuel Cell Systems (FCSs)

This subsection analyzes the role that stationary fuel cell systems (FCSs) can play in meeting California's carbon dioxide (CO_2) emission reduction targets. Complete historical data series are identified for CO_2 emissions from electric power plants in California. Based on this complete baseline data, historical changes in CO_2 emissions are described for California by region over time. Descriptions are included for segments of the California electricity sector to replace with FCSs with the goal of reducing CO_2 emissions. This subsection analyzes expected changes in CO_2 emissions for different FCS types, designs, and control strategies. This information is summarized further in the peer-reviewed conference proceedings of Reference 3.

The U.S. wastes one-fifth of its total energy consumption, 21 Quadrillion British Thermal Units (Quads), as heat at power plants, and then regenerates approximately this same amount downstream to heat buildings and industry. If traditional, centralized electric power production were replaced with high-efficiency, low-emission, decentralized, cogenerative power plants, the U.S. could reduce its energy consumption by up to one-fifth [4]. While the average U.S. electric power plant operates with an efficiency of about 32%, distributed generators achieve efficiencies as high as 90% (combined electrical and thermal). These distributed generators can be located close to buildings so that their heat can be recovered for building space and hot water heating [5]. By contrast, centralized generation is typically located far from population centers, not close to sources of thermal demand. One type of high-efficiency, low-emission distributed generator is the stationary cogenerative (or combined heat and power [CHP]) FCS [6].

Of all distributed generators, this research focuses on FCSs for several reasons. FCSs have higher electrical efficiencies, lower GHG emissions (carbon dioxide [CO_2], methane [CH_4], etc.), and lower air pollutant emissions (sulfur oxides [SO_x], nitrogen oxides [NO_x], carbon monoxide [CO], particulate matter [PM], etc.) than all other types of distributed generators consuming the same fuels [4, 7, 8, 9]. By contrast, microturbines fueled by natural gas have very low electrical efficiencies (around 20%) and higher air pollution emissions than FCSs fueled by the same fuel. Similarly, internal combustion engine systems fueled by natural gas have a relatively low electrical efficiency (around 30%) and higher air pollution emissions than FCSs, as well as noise abatement and maintenance concerns.

CHP FCSs can provide electricity and heat to buildings with lower GHG emissions than other generators if the CHP FCSs are well-designed and optimally dispatched. A key factor impacting their ability to reduce GHG emissions is the way they are controlled. Any CHP system may produce electricity and heat in excess of the amount that can be usefully consumed by surrounding buildings and other applications. By contrast, if optimally configured for reducing either GHG emissions or costs, CHP FCSs will be designed and dispatched so that a large portion of the electricity and heat that they produce is consumed in buildings or for useful purposes. Both the relationship between the amount of electricity produced by the CHP FCSs to that consumed and the relationship between the quantity of heat produced by CHP FCSs to that

consumed strongly impact the degree to which CHP FCSs reduce (or increase) GHG emissions compared to other generators [3, 4, 7, 8, 10]. If CHP FCSs were configured such that all of their heat and electricity were consumed, they could displace a significant quantity of GHG emissions [11]. For example, compared with conventional power and heat generation, CHP FCSs fueled by natural gas can reduce CO_2 emissions by 65% or more, if they are designed and controlled with perfect in-use electricity and heat capacity utilizations [4]. In-use energy capacity utilization (of electricity or heat) can be defined as the ratio of the energy produced by the FCS that is usefully consumed as an end-product to the FCS's maximum energy output. If CHP FCSs are fueled by renewable hydrogen (H_2), they release approximately no net CO_2 emissions [3].

1.2. Optimizing the Design of CHP FCSs

Energy system optimization models investigate 12 novel operating strategies for CHP FCSs composed of various operating configurations. Most FCSs are now installed as stand-alone, fixed heat-to-power ratio (FHP), and no load following. Systems can be, however, configured as heat load following, electricity load following, or no load following. Load following the electrical demand results in by-product heat, and vice versa, while no load following is independent of demand and is generally constant. When load following, the system is physically constrained by the energy output range and ramp rate (the ability to change electrical output in a given amount of time). Systems can also be configured with a fixed or a variable heat-to-power ratio (VHP). Changing to a VHP will increase the systems load following operating range. This section is discussed further in the peer-reviewed conference proceedings of References 12, 13, and 14.

Novel strategies are examined using simulation tools. Models evaluate novel operating strategies for stationary FCSs installed in buildings. Models optimize the percentage installation of FCS for minimum CO_2 emissions, minimum CO_2 emissions per unit energy cost, or maximum energy cost savings to building owners. Models also optimize FCS installations for a particular location, climatic region, building load curves, FCS type, and competitive environment. Models shows trade-offs among competing goals: cost savings to building owners, CO_2 reductions, FCS installed capacity, and manufacturer sales.

Models include 2007 real-time measured demand data for electricity, steam, and chilled water from 19 Stanford buildings at one-hour time increments. A unique feature of this data set is that the space cooling demand is directly measured and distinguishable from electricity demand (unlike air-conditioning systems). The four seasons are represented using four weeks of measured data with similar weather conditions to the seasonal averages (avoiding school breaks). Selected weeks are chosen to have a dry bulb temperature within 0.5 standard deviations of the seasonal average.

Our energy system optimization models evaluate novel FCS operating strategies, not typically pursued by commercial industry. Most FCSs today are installed according to a "business-as-usual" approach: (1) stand-alone (unconnected to district heating networks and low-voltage electricity distribution lines), (2) not load following (not producing output equivalent to the instantaneous electrical or thermal demand of surrounding buildings), (3) employing an FHP (producing heat and electricity in a constant ratio to each other), and (4) producing only electricity and no recoverable heat. By contrast, our models consider novel approaches as well.

Novel approaches include (1) networking (connecting FCSs to electrical and/or thermal networks), (2) load following (having FCSs produce only the instantaneous electricity or heat demanded by surrounding buildings), (3) employing a VHP (such that FCSs can vary the ratio of heat and electricity they produce), (4) cogeneration (combining the production of electricity and recoverable heat), (5) permutations of these together, and (6) permutations of these combined with more ―business-as-usual" approaches.

Many peer-reviewed publications discuss models that investigate CHP FCS thermodynamic operation [15, 16, 17]. Some articles present for the first time models optimizing the control of a Proton Exchange Membrane (PEM) FCS's anode off-gas burner [16] and the concept of a VHP [17]. Other peer-reviewed publications discuss models that evaluate the economics and environmental impacts of deploying stationary CHP FCSs within the context of real-time electricity and heating demands [4, 18, 19, 20, 21, 22, 23].

1.3 Optimizing the Design of Combined Cooling, Heating, and Electric Power (CCHP) FCSs

Energy system optimization models investigate novel operating strategies for CCHP FCSs. CCHP or tri-generative FCSs can convey electricity, recoverable heat, and chilled water to multiple buildings via networks. FCSs can be configured to convert unrecovered heat into cooling power with an absorptive cooling cycle (ACC). Chilled water production can be included in FCS operation with devices such as single, double, and triple effect lithium bromide (LiBr) absorption chillers [24]. Unrecovered heat from FCSs supplies the energy needed for the chiller's generator. This information is summarized further in the peer-reviewed conference proceedings of References 25 and 26.

The following describes the single-effect LiBr ACC, or chiller. This is the standard cycle for producing chilled water from low-temperature heat of ~95 °C. The double-effect LiBr cycle offers improved performance for higher-temperature heat of ~135 °C at the expense of a more complex cycle, while the ammonia cycle allows the production of ice with heat around ~135 °C.

A basic ACC, shown in Figure 1, uses high temperature heat (Q_G) to generate a refrigerant in a boiler, condenses the refrigerant by transferring heat (Q_C) to the medium temperature environment, evaporates the refrigerant at reduced pressure to absorb heat (Q_E) from the low-temperature cooling load, and absorbs the refrigerant in the concentrated solution where heat (Q_A) is removed to the medium-temperature environment before the now dilute solution is sent back to the generator to repeat this cycle.

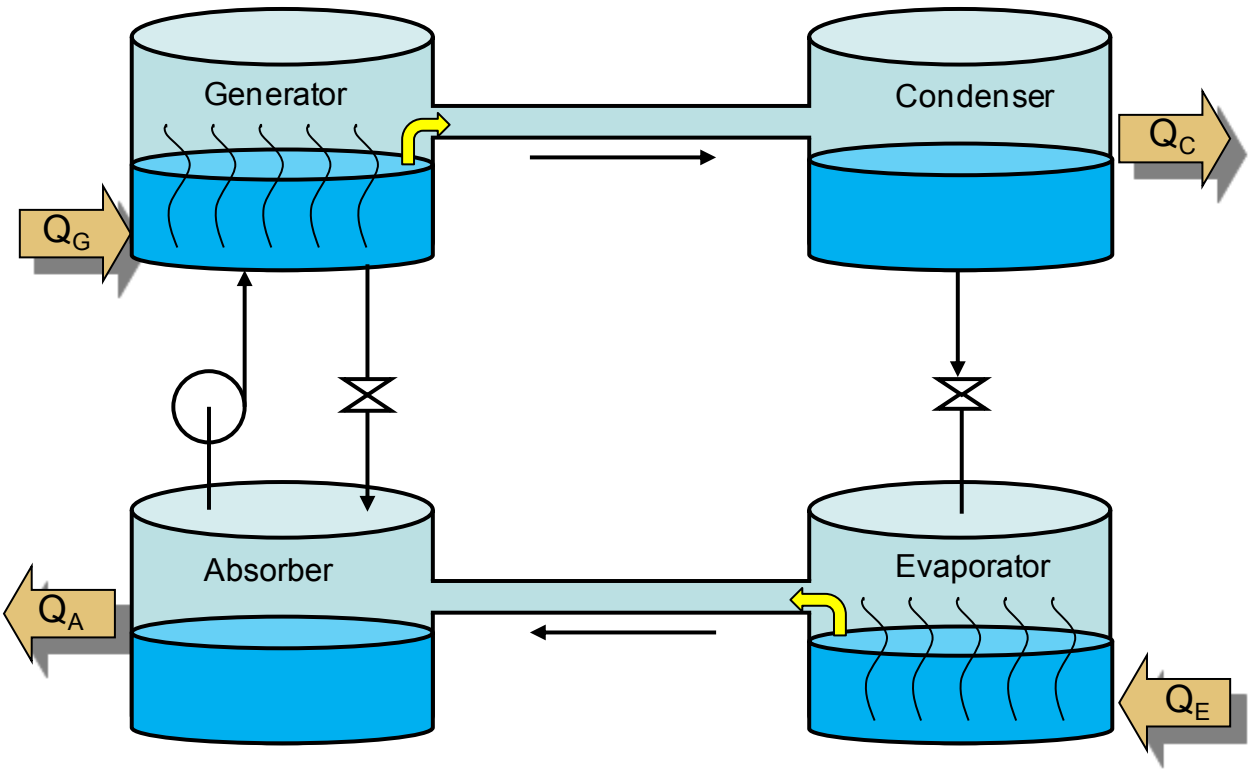

Figure 1. Absorptive cooling cycle (ACC).

Although traditionally, absorption chillers have been integrated with gas turbines to produce CCHP, FCSs can also be used to drive ACCs using high-quality unrecovered FCS heat. Commercial absorptive cooling systems are usually large for two principal reasons: (1) the economy of scale for large units, and (2) these systems operate at a lower coefficient of performance (COP) than electric chillers. COP is defined as the quantity of cooling power output divided by either heat input (for absorption chillers) or electricity input (for electric chillers). Due to the lower COP, absorption chillers are usually associated with either large unrecovered heat streams, or applications where high electricity prices make it economical to replace a large demand for electric cooling with thermally driven absorptive cooling supply.

Models developed here realistically describe the engineering performance of CCHP FCSs and competing generators. Models assume a one megawatt of electrical power (MWe) Molten Carbonate Fuel Cell (MCFC) system based on units currently in production at FuelCell Energy, Inc. (FCE). CCHP MCFC performance is tested against that of CHP combined cycle gas turbines (CCGT) while competing cooling generator COP values are based on measured operating data over absorption and electric chiller load cycles. Financial and operating data are realistically described for CCHP FCSs, competing generators, and energy storage capabilities.

1.4. Thermodynamic and Chemical Engineering Models of CCHP FCSs

Models developed here realistically describe the thermodynamics and chemically engineering design of a double-effect LiBR CCHP FCSs over a range of operating conditions. Models

thermally integrate LiBR heat demand with FCS heat supply. Models analyze the performance of novel CCHP FCSs over a range of conditions. This information is summarized further in the peer-reviewed conference proceeding of Reference 27.

Single-effect LiBr chillers absorb heat between 80 and 110 °C and generate cooling power with a COP of between 0.5 and 0.7. A double-effect LiBr chiller absorbs higher-temperature heat between 120 and 150 °C and generates cooling power at a higher efficiency with a COP of between 0.8 and 1.2. Triple-effect LiBr chillers can potentially absorb heat at even higher temperatures and produce cooling at higher COP.

The thermodynamic processes of a single effect, basic ACC can be seen in Figure 1 and are described in greater detail below:

Generator – Heat (Q_G) is added to a generator to boil the refrigerant out of a solution. The concentrated solution is sent to an absorber via an expansion valve, and the refrigerant vapor is sent to a condenser.

Condenser – The gaseous refrigerant is condensed and cooled by removing some of its heat (Q_C) to the environment. This heat may also be applied to a medium-temperature heat sink (such as a hot water load). The condensed and cooled liquid refrigerant is sent through an expansion valve to an evaporator.

Evaporator – Heat (Q_E) is removed from a low-temperature cooling load through the evaporation of the liquid refrigerant. This gaseous refrigerant travels to the absorber.

Absorber – The gaseous refrigerant is absorbed into the concentrated solution, and heat (Q_A) is removed to the environment or a medium-temperature heat sink, such as a hot water load. The resulting less-concentrated solution is pumped to the generator to close the refrigerant cycle.

2. Methodology

2.1. Potential GHG Impact of Stationary FCSs

A theoretical analysis was conducted to examine the effect on GHG emissions of displacing historical California electricity generation with FCSs. The study examines the hypothetical effect of replacing energy production from California power plants over a 15-year period (1990 to 2004) with that from different types of FCSs. The study reports the cumulative changes in CO_2 emissions over the 15-year period. Under an idealized scenario, it is assumed that FCSs:

1. do not operate cogeneratively (they produce only electricity, and not recoverable heat),
2. are electrically networked into the surrounding low-voltage distribution grid,
3. do not follow the electrical load of surrounding buildings, and
4. operate steadily at a maximum electrical efficiency.

The following FCS types are evaluated: proton exchange membrane fuel cell (PEMFC), phosphoric acid fuel cell (PAFC), molten carbonate fuel cell (MCFC) and solid oxide fuel cell (SOFC). The maximum electrical efficiency of each system is assumed to be 32% for PEMFC, 37% for PAFC, 54% for a hybrid MCFC system with a downstream gas turbine, and 60% for a hybrid SOFC system with a downstream turbine. All are fueled by natural gas. These efficiency values are consistent with quoted performance from fuel cell manufacturers for either prototype or commercial systems demonstrated to date. There is some uncertainty in the wide-spread applicability of these assumed efficiencies, which are affected by how quickly FCS developers can commercialize best-available technologies.

Each of these fuel cell types is evaluated under three different cases:

1. The systems replace 100% of generation (both in-state and imported generation).
2. The systems replace all in-state generation.
3. The systems replace all imported electricity.

The change in CO_2 emissions over time by region is plotted. The first case is important for businesses in California that are interested in reducing their carbon footprint and want to know if it would be better for them to connect to the California grid or to install a FCS. The other cases are important for policy makers and engineers designing and facilitating the installation of these systems. Additional scenarios are also evaluated.

2.2. Optimizing the Design of CHP FCSs

Energy system optimization models investigate novel operating strategies for CHP FCSs. Models evaluate the efficacy of FCSs operating with novel fuel cell strategies, such as networking, VHPs, and load following constraints. A layout showing a schematic diagram of a CHP FCS is shown in Figure 2.

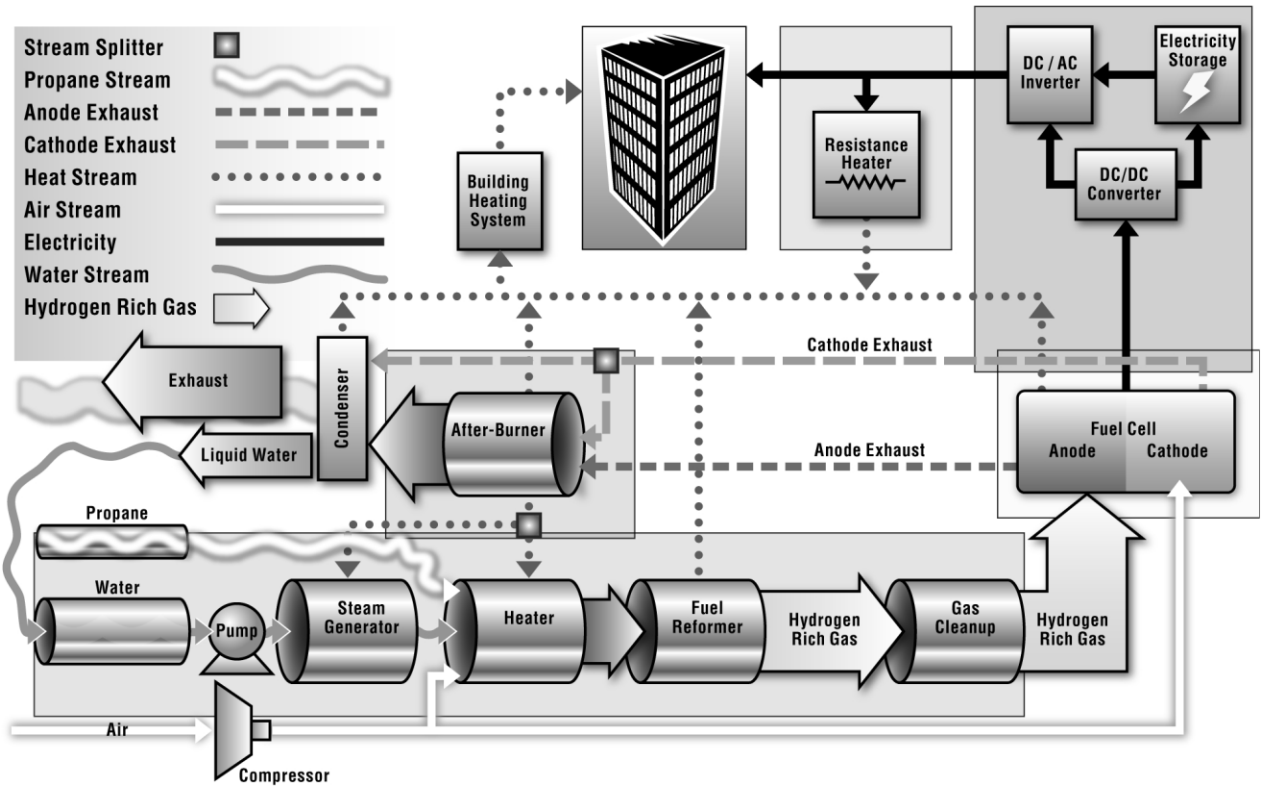

Figure 2. Fuel cell system layout (Redrawn from Reference 9, Figure 10.1, Page 281).

Energy system optimization models investigate novel operating strategies, including thermal and electrical networking. The FCSs can be installed as either stand-alone or networked. In networked scenarios, the FCSs are connected to the local electricity distribution grid and to district heating systems. In stand-alone scenarios, each FCS serves only one building. Hence, the FCSs cannot convey or sell excess heat or electricity into distribution networks to reach other buildings. Buildings can import additional heat and electricity from competing generation sources. During times of low energy demands for a building, the FCS can often be running at a lower capacity utilization because there is no way to distribute the energy it could be producing at maximum capacity to other buildings that may have additional energy demands at that time. The fuel cell companies FCE Inc., UTPower Inc., and Bloom Energy Inc. historically have installed their units in this way. By contrast, networked FCSs have access to energy distribution channels. In the models, networked FCSs are defined as being able to convey excess heat or electricity into distribution channels to reach other buildings, and are able to sell back excess electricity back to the regional grid. For networked approaches, low voltage electrical distribution grid losses are estimated at approximately 0%, and heat losses are estimated at

approximately 8%. In practice, thermal distribution losses can be a strong function of outside temperature. In practice, potential limitations in networking systems are that the transfer of energy among buildings and through networks would need to be managed, either through joint-ownership of resources or through agreed-upon standards for transactions. Furthermore, the infrastructure for electrical and thermal networks tends to already exist in niche markets, primarily found at U.S. universities, in European towns, and in highly-populated urban areas. Where infrastructure does not already exist, investment in new infrastructure requires high initial capital investment. This investment can be profitable, but may require a longer pay-back period than some investors are willing to bear. Figure 3 shows visually the difference between stand-alone (S) and networked (N) FCSs. The figure contrasts the stand alone case where FCSs are not connected to electrical, thermal and cooling distribution networks, and, the networked case, where FCSs are connected to these networks. Cooling distribution networks are discussed in the subsequent section.

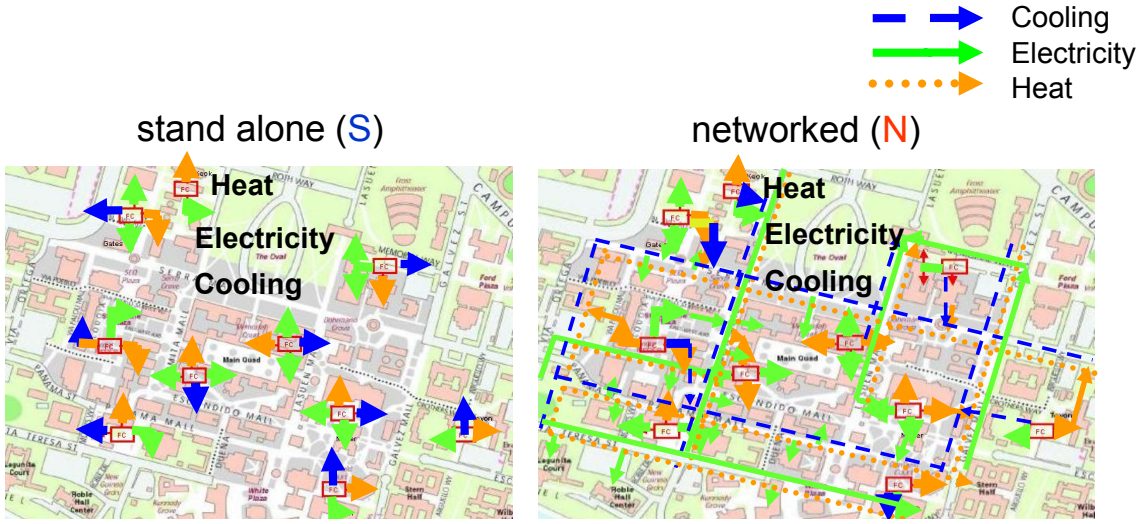

Figure 3. Cooling, electricity, and heat flow in stand-alone vs. networked FCSs.

Energy system optimization models investigate novel operating strategies, including variable heat-to-power ratio. FCSs can be installed with either an FHP or with a VHP. Historically, UTC Power Inc. and FCE Inc. [28] have installed most of their co-generative FCSs with a FHP, although FCE Inc. has enabled VHP as an add-on design feature with some installations. In contrast to U.S. manufacturers, Japanese manufacturers, such as Toho GAS Co., Ltd. and the Swiss manufacturer, Hexis Ltd., are building most of their systems with VHP capability. A VHP enables a FCS to rapidly change the ratio of heat recovered to the amount of electricity it produces. One way VHP capability can be achieved is by designing an FCS to intentionally decrease its net electrical efficiency from its maximum.

Systems can be configured with a VHP using a variety of methods. These methods are shown in the separate boxed areas of Figure 2. One method is to vary the ratio of reactants, the temperature, and/or the pressure in the fuel processing subsystem to alter the energy consumed or released by the fuel reforming reactions, and to alter the amount of fuel flowing to the fuel cell, and the heat it releases. Another option is to vary the fuel flow rate to the anode off-gas burner. A third method is to vary the system's electrical configuration while a fourth method is to change the shape and/or position of the polarization curve during operation. An additional option is to use a resistance heater, but this approach increases cell run time and could potentially increase cell degradation and decrease lifetime.

The model describes electricity, heating, and cooling demand, which vary by time of day, day of week, season, and building type. The model also describes the financial and operating data for FCSs and competing generators. Electricity demand for five buildings is shown in over a one-week period.

Models include 2007 real-time measured demand data for electricity and steam from 19 different Stanford University buildings at one hour increments [29]. Models describe electricity and heating demand for multiple buildings, which varies by time of day, day of week, and season. Figure 4 shows example data from the model for electricity demand over a one week time period in winter for five different buildings from five different building categories. Building categories are based on the purpose of the building, and include dry laboratories, wet laboratories, computing facilities, museums/libraries, and other buildings. Demand data from 19 different Stanford University buildings measured in calendar year 2007 was scaled up to simulate total campus demand through a detailed technique.

Models analyze a range of incentives and carbon taxes that affect total cost savings to the building owner. The carbon tax values investigated, in \$/tonne of CO_2 emitted, are \$0, \$20 and \$100. Some of our key assumptions are that the base case equals no fuel cells; all generators are CHP CCGT plants; the common fuel for fuel cells and turbines is natural gas; the base case electricity and heating costs (no fuel cells) is \$40 million/yr; the networked model is able to sell back to grid at purchase price; the cost of capital is 7.42%, which is the educational borrowing rate; and the fuel cell turn-key cost (without incentives) is \$4,300/kWe (kilowatt of electrical power). Fuel cell incentives are \$2,500/kWe (state) and \$1,000/kWe (federal). Free market price of natural gas is \$8.95/million BTU (British Thermal Units) and natural gas price with CHP incentive of \$7.45/million BTU.

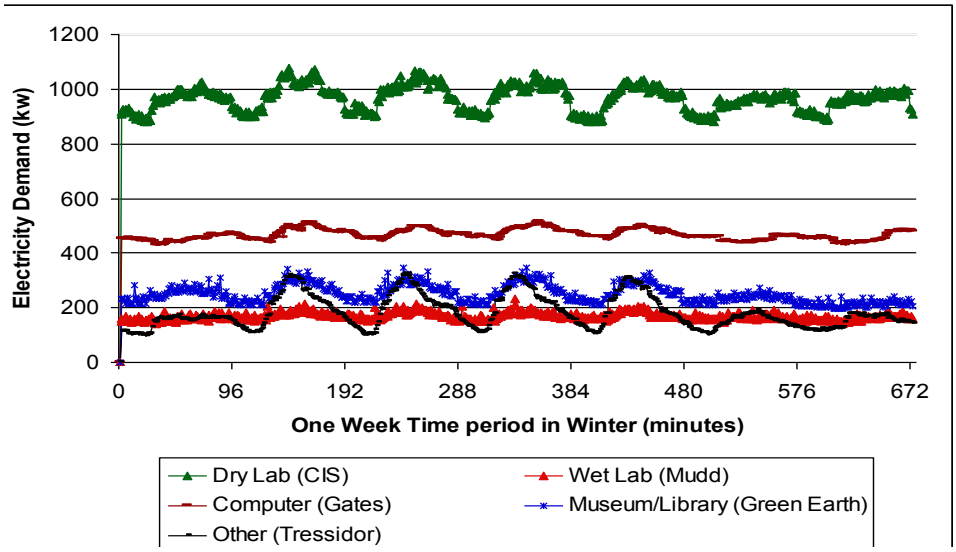

Figure 4. Electricity demand curves for five buildings on the Stanford University campus over a one-week period.

Models investigate 12 novel operating strategies, summarized below in Table 1. Most FCSs are now installed according to Strategy 1 [SFEXHN], or stand-alone, fixed/variable heat-to-power ratio, maximum electrical output, and minimum heat output.

Table 1. Fuel Cell System Operating Strategies Investigated.

			Primary Control	Secondary Control
Strategy	Electrically and Thermally Networked (N) or Stand Alone (S)?	Variable Heat-to-Power Ratio (V) or Fixed Heat-to-Power Ratio (F)?	Electricity Power Load Following (E), Heat Load Following (H), or No Load Following (EX)?	Electricity Power Load Following (E), Heat Load Following (H), or No Load Following (HN, HX, EN, EX)?
1	S	F	EX	HN
2	S	V	H	E
3	S	V	EX	H
4	N	F	E	HN
5	N	F	E	HX
6	N	F	EX	HN
7	N	F	EX	HX
8	N	V	H	EN
9	N	V	H	E
10	N	V	E	H
11	N	V	H	EX
12	N	V	EX	H

2.3. Optimizing the Design of CCHP FCSs

Models examine novel operating strategies not common in commercial industry. Novel approaches include thermal and electrical networking (N); variable heat-to-power ratio (V); tunable cooling-to-heat output; and cooling, electricity, or heat load following (C, E, or H). Models also optimize the installed capacity of CCHP FCSs and the installed capacity of cooling, thermal, and electrical energy storage for either minimum CO_2 emissions, or maximum combined energy cost savings for building owners in using cooling power, heat, and electricity compared with competing technologies. Models test CCHP FCSs against real-time demand data for electricity, steam, and cooling power. Demand data is measured in real-time every hour in a year from 19 different buildings. Models minimize the total yearly costs for building energy provision. Total yearly building energy costs include, but are not limited to, the FCS capital, maintenance, and fueling costs as well as the competing generators' electricity, heating, and cooling costs. All demand not supplied by an FCS is purchased from the competing generators.

Models also evaluate multiple permutations of market conditions such as incentives, various carbon taxes, grid sellback, fixed or variable electrical pricing, and different demand curves. Models include real-time electricity pricing based on measured data from competitive electricity markets such as those in Europe. Models also evaluate multiple permutations of engineering designs such as storage capabilities for electricity, thermal, and cooling and a COP of 0.5, 1, or 2. Models evaluate eight novel operating strategies investigated, labeled i-viii in Table 3. A number of novel operating strategies are investigated with primary, secondary, and tertiary controls for H_2, electricity, and heat load following.

Models are automated with Visual Basic macros that reduce computing time and labor-hours, and increase available data. The optimization macro uses a low-precision, broad search and a high-precision, detailed search to find optimal energy storage capacity (electricity, heat, and cooling storage) and optimal FCS installation capacity. First, the broad search estimates optimal storage capacities for all possible FCS installed capacities. Second, using the estimated storage values from the broad search, the detailed search focuses to within a 10% tolerance range of the broad search's cost or CO_2 optima. For both searches, the algorithm optimizes for the most economical storage type to the least economical type (thermal storage, followed by cooling storage, and then electrical storage.)

A FCS uses a cooling-to-heat ratio that reflects the physics of converting FCS heat to a chilled water stream with an absorption chiller or another thermodynamic cycle. A FCS with tunable cooling-to-heat output can convert thermal energy into cooling power over a certain range. The maximum cooling production rate (C) is limited to the product of its COP and the maximum heat production rate (Q) from the FCS; this relationship is illustrated for different COPs in Figure 5.

$$C = COP \times Q \tag{1}$$

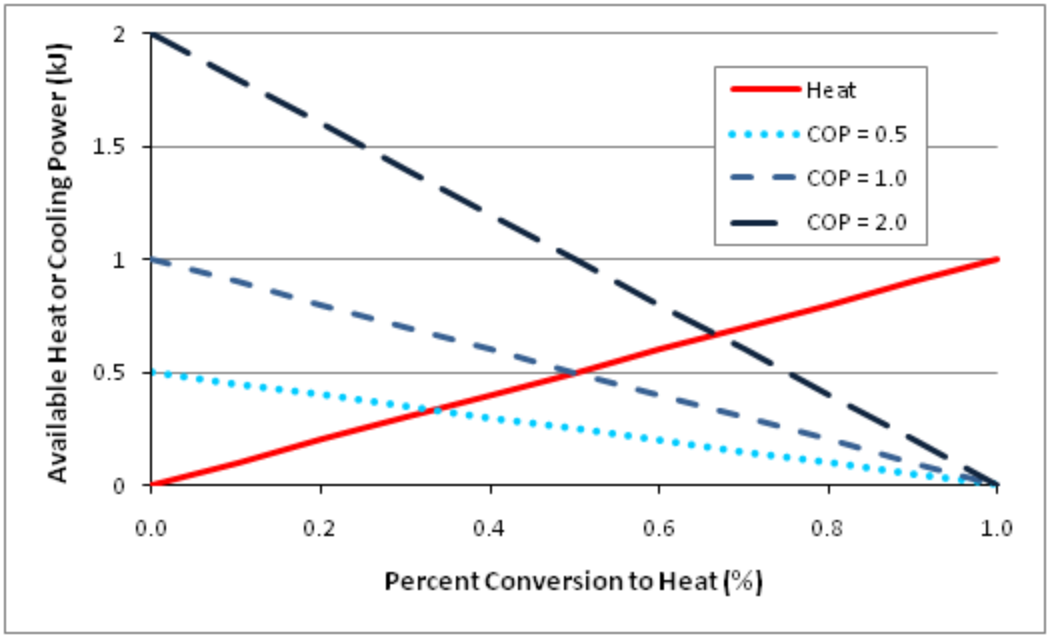

Figure 5. Cooling production with varying heat production.

Models evaluate multiple permutations of market conditions. Models evaluate permutations where FCSs can sell back electricity to the grid at the same price that the competing electricity generator charges (similar to net-metering but without a constraint on the total quantity of electricity sold back to the grid per year), at 25% of the purchase price, or not at all.

- Various permutations were considered for the model, allowing the user to specify which conditions they would like to model and allowing the results to match the financial market, environment, and particular situation being modeled.
- Incentives specify whether or not there are federal or state subsidies available for the installation of an FCS. A range of carbon taxes influences the energy commodity prices based on the levels of GHG that they emit. The grid sellback feature determines whether or not an FCS can sell electricity back to the grid for a profit if electrical energy production exceeds demand.
- The model also allows either fixed or market (real-time) electricity pricing to be used. Furthermore, it is possible to set a range of electricity sellback prices, currently set at either 25% or 100% of the purchase price. Finally, the original demand curves for various energy types can be reversed in order to see the effects of different load curves.
- Models include real-time electricity pricing based on measured data from competitive electricity markets. The methodology related to simulating the real-time electricity price is given by Huisman [30]. Given that the electricity pricing in some markets can vary tremendously from one time of day to another, it is useful to be able to analyze scenarios with a changing electrical price rather than only using a constant price.
- Models evaluate multiple permutations of engineering designs. Models evaluate multiple engineering strategies for installation, design, and control. Models have the ability to turn on and off storage capabilities for various energy types to determine whether or not they are cost-effective or help reduce GHG emissions.

- Models consider a range of COPs for the CCHP FCS. Current model assumptions are no added cost to increase COP.
- A matrix of permutations for cost optimization is evaluated using the models as shown in Table 2. Table 2 summarizes the permutations considered; each highlighted column represents one of the permutation considerations taken when specifying the conditions of a certain situation. The columns refer to market and engineering performance conditions.

Table 2. Table of Scenario Permutations.

	Incentives (Y/N)	Carbon Tax ($0, $20, $100 /ton CO2)	Grid Sellback (Y/N)	Electrical Price (Fixed/ Market)	Sellback Price (Full/ 25%)	Demand (Original/ Reversed)	Storage Capacity (Y/N)	Coefficient of Performance (0.5, 1, 2)
I	Y	0	Y	F	F	O	N	0.5
II	Y	0	Y	F	F	O	Y	0.5
III	Y	0	N	F	F	O	Y	0.5
IV	Y	0	N	M	F	O	Y	0.5
V	Y	0	Y	M	F	O	Y	0.5
VI	Y	20	Y	F	F	O	N	0.5
VII	Y	20	Y	F	F	O	Y	0.5
VIII	Y	20	N	F	F	O	Y	0.5
IX	Y	20	N	M	F	O	Y	0.5
X	Y	20	Y	M	F	O	Y	0.5
XI	Y	100	Y	F	F	O	N	0.5
XII	Y	100	Y	F	F	O	Y	0.5
XIII	Y	100	N	F	F	O	Y	0.5
XIV	Y	100	N	M	F	O	Y	0.5
XV	Y	100	Y	M	F	O	Y	0.5
XVI	Y	100	N	F	F	O	N	0.5
XVII	Y	100	Y	M	F	O	N	0.5
XVIII	Y	100	N	M	F	O	N	0.5
XIX	Y	100	Y	F	F	O	N	1
XX	Y	100	Y	F	F	O	Y	1
XXI	Y	100	N	F	F	O	Y	1
XXII	Y	100	N	M	F	O	Y	1
XXIII	Y	100	Y	M	F	O	Y	1
XXIV	Y	100	N	F	F	O	N	1
XXV	Y	100	Y	M	F	O	N	1
XXVI	Y	100	N	M	F	O	N	1
XXVII	Y	100	Y	F	F	R	N	1
XXVIII	Y	100	Y	F	F	R	Y	1
XXIX	Y	100	N	F	F	R	Y	1
XXX	Y	100	N	M	F	R	Y	1
XXXI	Y	100	Y	M	F	R	Y	1
XXXII	Y	100	N	F	F	R	N	1
XXXIII	Y	100	Y	M	F	R	N	1
XXXIV	Y	100	N	M	F	R	N	1
XXXV	Y	100	Y	F	F	O	N	2
XXXVI	Y	100	Y	F	F	O	Y	2
XXXVII	Y	100	N	F	F	O	Y	2
XXXVIII	Y	100	N	M	F	O	Y	2
XXXIX	Y	100	Y	M	F	O	Y	2
XXXX	Y	100	N	F	F	O	N	2
XXXXI	Y	100	Y	M	F	O	N	2
XXXXII	Y	100	N	M	F	O	N	2
XXXXIII	Y	100	Y	F	25%	O	N	0.5
XXXXIV	Y	100	Y	F	25%	O	Y	0.5
XXXXV	Y	100	N	F	25%	O	Y	0.5
XXXXVI	Y	100	N	M	25%	O	Y	0.5
XXXXVII	Y	100	Y	M	25%	O	Y	0.5
XXXXVIII	Y	100	N	F	25%	O	N	0.5
XXXXIX	Y	100	Y	M	25%	O	N	0.5
XXXXXX	Y	100	N	M	25%	O	N	0.5

The model investigates eight novel operating strategies shown in Table 3. Strategies i to viii are all electrically and thermally networked (N), with a variable heat-to-power ratio (V). A number of novel operating strategies are investigated with primary, secondary, and tertiary controls for cooling, heating, and electricity load following. Most FCSs are now installed as SFEXHN.

Table 3. List of FCS Operating Strategies Considered.

				Primary Control	Secondary Control	Tertiary Control
Strategy	Electrically, Thermally and Cooling Networked (N) or Stand Alone (S)?	Variable Heat-to-Power Ratio (V), Fixed Heat-to-Power Ratio (F)?	Tunable Cooling to Heat Output (T)?	Electricity Power Load Following (E), or No Electricity Load Following (EX)?	Heat Load Following (H), Cooling Load Following (C), No Heat Load Following (HN, HX)?	Heat Load Following (H), Cooling Load Following (P), No Heat Load Following (HN, HX)?
i	N	F	T	E	HN	C
ii	N	V	T	E	C	HX
iii	N	F	T	EX	HN	C
iv	N	V	T	EX	C	HX
v	N	V	T	E	H	C
vi	N	V	T	E	C	H
vii	N	V	T	EX	H	C
viii	N	V	T	EX	C	H

- Table 3 shows each of the FCS operating strategies simulated, labeled i-viii.
- Each strategy considered in this analysis is assumed to be networked with a variable heat-to-power ratio (V) and a tunable cooling-to-heat output (T).
- Each strategy then has a primary, secondary, and tertiary control whereby the FCS attempts to meet energy demand in that order. Electricity, either with load following (E) or without load following (EX), is always the primary control due to model constraints because thermal and cooling energy production are based off of electrical output. The secondary and tertiary controls are cooling load following (C), heat load following (H), minimum heat production (HN), or maximum heat production (HX).

2.4. Thermodynamic and Chemical Engineering Models of Combined Cooling, Heating, and Electric Power

A steady-state SOFC model has been developed in AspenPlus™. The model uses the polarization equations based on Shaffer and Brouwer [31]. FCS exhaust gas flow rate, composition, temperature, specific heat and pressure are determined for different fuel cell operating parameters such as fuel utilization and current density. The exhaust gas stream is introduced to the chiller as the main input. In certain scenarios, the integration of the fuel cell and chiller models incorporates the capability of blending the fuel cell exhaust gas with ambient air to control the chiller input temperature while maintaining a high mass flow rate to the chiller. In addition, parasitic loads associated with fuel and air compression and water pumping are calculated with the model.

ABSORPTION CHILLER MODEL

The system modeled is a double-effect absorption chiller that uses LiBr-H_2O solution as the working fluid where water is the refrigerant and LiBr-H_2O is the absorbent. The chiller model is a steady-state model that uses the thermodynamic properties of the LiBr-H_2O solution based on Reference 32. An extensive calculator block embedded in AspenPlus™ has been incorporated to simulate the chiller.

2.4.1. Modeling Combined Cooling, Heating, and Electric Power Fuel Cell Systems

Models simulate advanced CCHP FCSs in AspenPlus™. A flowsheet showing one version of a schematic diagram of the AspenPlus™ model can be seen in Figure 6. The colored lines represent material or heat streams, used to physically model the thermodynamic processes present in the CCHP system. Modeling calculations are performed directly through AspenPlus™ as well as through linked Excel spreadsheets, containing lookup tables and more complex calculations. Sensitivity studies within AspenPlus™ are used to produce large amounts of data over the ranges of operation of both fuel cell and chiller.

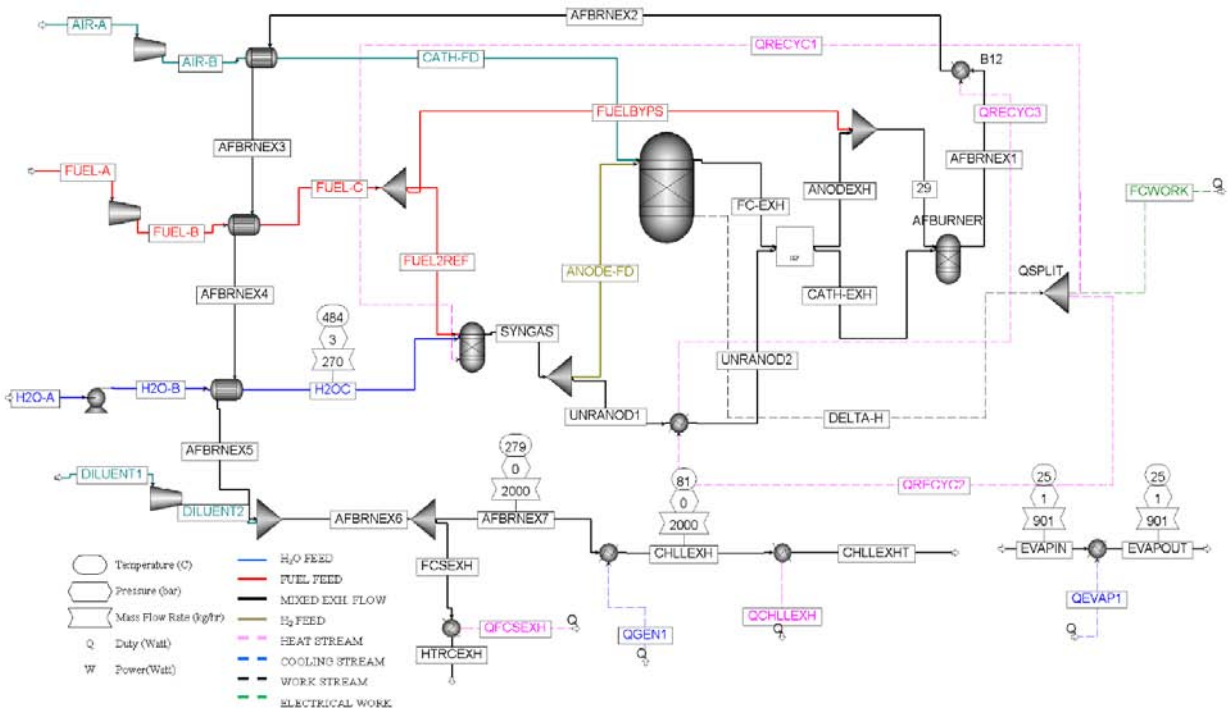

Figure 6. Schematic of AspenPlus™ CCHP model.

The models use polarization expressions and constants from the peer-reviewed literature and from industry. This conceptual model is analyzed theoretically through thermodynamic models as well as through chemical engineering process plant flowsheet simulation using AspenPlus™ software. The total heat released by the fuel cell stack and subsystem, in kilojoules (kJ), is shown in Equation (2).

$$Q_{FC} = \Delta H_{rxn,fc} - W_{elec} \tag{2}$$

where

Q_{FC} = Total heat released by the fuel cell stack and subsystem, (kJ),
$\Delta H_{rxn,\,fc}$ = Heat of reaction for the oxidation of H_2 and/or CO within the fuel cell stack (kJ), according to the reactions $H_2 + ½\ O_2 \rightarrow H_2O$ and/or $CO + ½\ O_2 \rightarrow CO_2$, and
W_{elec} = electric work output of the fuel cell stack, (kJ).

The electric work output from the fuel cell stack is related to electrical potential from the fuel oxidation reaction. The reversible, maximum work (W_{elec}^{ideal}) generated by the fuel cell is based on Gibbs free energy of reaction [$\Delta G_{rxn}(T)$] and is proportional to the ideal voltage V^{ideal}.

$$W_{elec}^{ideal} = n_e F V^{ideal} \tag{3}$$

$$V^{ideal} = \frac{\Delta G_{rxn}(T)}{n_e F} - \frac{R_u T_{out}}{n_e F} \ln K \tag{4}$$

V^{ideal} is the ideal voltage, and is directly related to the temperature-dependent Gibbs free energy as well as the equilibrium constants for the oxidation reaction.

K = chemical reaction equilibrium constant.
R_u = Universal Gas Constant, (0.08205 L atm/mol/K).
n_e = number of electron transferred during the oxidation process.
F = Faraday constant (96,486 C/mol).
T_{out}= temperature.

In reality, the electrochemical potential is far from ideal due to polarization losses. The three losses that need to be calculated are loss due to activation of chemical reactions (η_{act}), loss due to internal ohmic resistance (η_{ohm}), and loss due to concentration gradient (η_{conc}).

$$W_{elec} = n_e F V \tag{5}$$

$$V = V^{ideal} - \eta_{act} - \eta_{ohm} - \eta_{conc} \tag{6}$$

Each of the loss terms degrades the fuel cell performance by a different mechanism: concentration gradient, electrolyte material conduction, and electrode resistance. In this derivation, the loss calculations are based on the work of Shaffer, Hunsuck, and Brouwer [33]. For example, activation, ohmic, and concentration polarization are described according to

$$\eta_{act} = \frac{R_u T_{out}}{n_e F} \sinh^{-1}\left(\frac{j}{2j_{o,*}}\right) \tag{7}$$

where

$$j_{o,anode} = \gamma_{anode}\left(\frac{p_{H_2}}{p_{amb}}\right)\left(\frac{p_{H_2O}}{p_{amb}}\right)\exp\left(-\frac{E_{act,anode}}{R_u T_{out}}\right) \tag{8}$$

$$j_{o,cathode} = \gamma_{cathode}\left(\frac{p_{O_2}}{p_{amb}}\right)^{0.25}\exp\left(-\frac{E_{act,cathode}}{R_u T_{out}}\right) \tag{9}$$

and

$$\eta_{ohm} = i \times \left(R_{anode} + R_{cathode} + R_{IC} + R_{electrolyte}\right) \tag{10}$$

$$\eta_{conc} = -\frac{R_u T_{out}}{n_e F}\ln\left(1 - \frac{j}{j_L}\right) \tag{11}$$

where

$E_{act,*}$ = activation energy for activation polarization in anode or cathode,
i = current generated from the fuel stack (A),
j = current density (A/m^2),
$j_{o,*}$ = exchange current density at cathode and at anode (A/m^2),
j_L = limiting current density (A/m^2),
p_i = partial pressure of the i^{th} component. i = *ambient*, O_2, H_2O, and H_2,
R_k = ohmic resistance of k^{th} material. k = *anode, cathode, interconnect, and electrolyte*, and
γ_* = pre-exponential constant for activation polarization in anode or cathode.

Utilizing polarization constants of previously modeled SOFC systems by Shaffer et al. [33], voltage and power density curves for four different temperatures have been plotted in Figure 7. The voltage and electrical efficiency increase with increasing temperature but decrease with increasing current density.

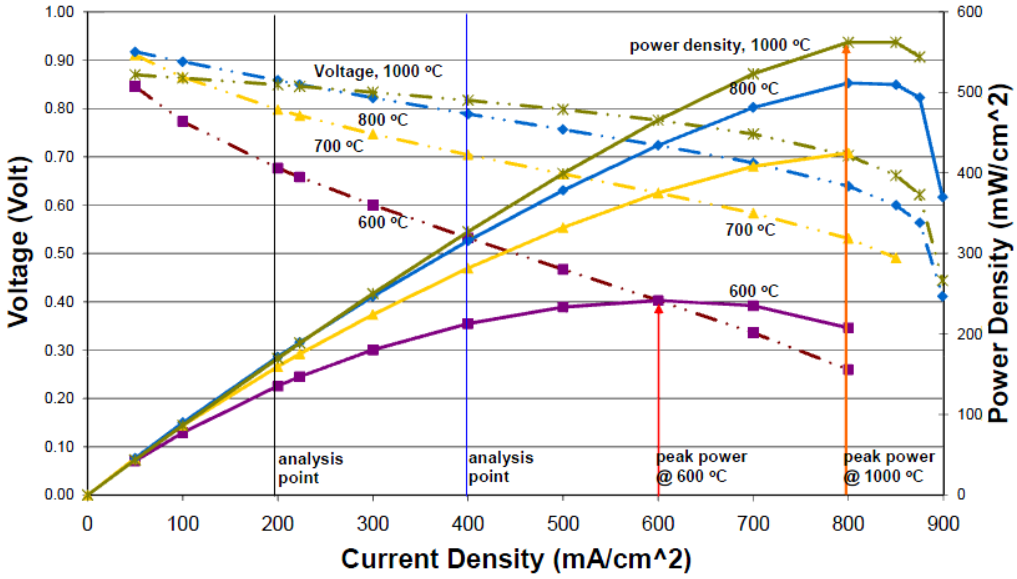

Figure 7. Fuel cell voltage and power density vs. current density.

2.4.2. Modeling Lithium Bromide Absorption Chillers

Advanced double-effect LiBr absorption chillers are modeled within AspenPlus™ CCHP FCS models. These chiller models realistically describe the thermodynamics of a LiBr double-effect chiller [34]. A schematic of the chiller is shown in Figure 8, and these numbered state points are used in the equations that follow.

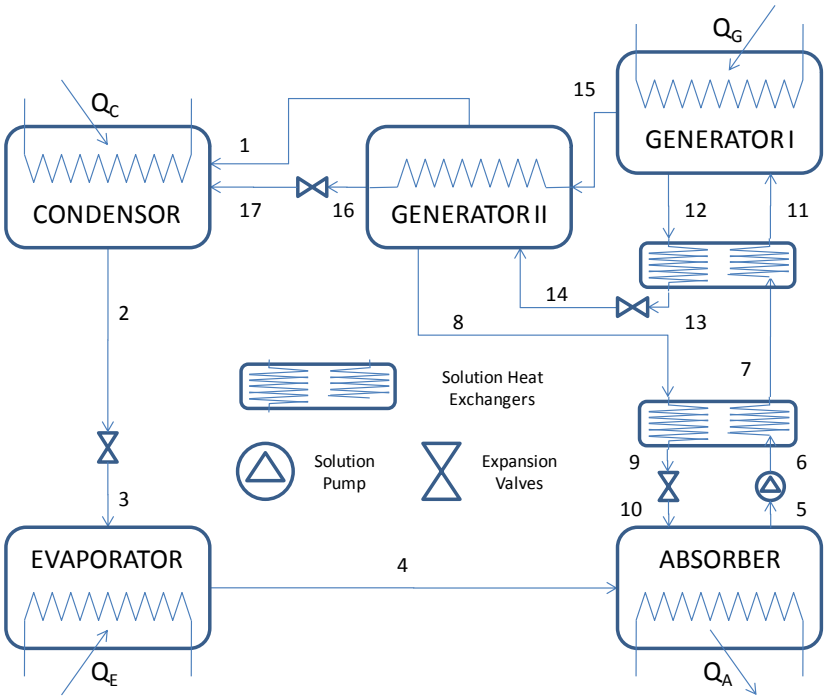

Figure 8. Double-effect LiBr/water absorption chiller schematic with state points.

Below is a numbered stream description for Figure 8 where gas/liquid corresponds to refrigerant and weak/med/strong corresponds to the concentration of LiBr-water solutions:

1 - gas – From Generator II to Condenser
2 - liquid – From Condenser to Evaporator Expansion Valve
3 - liquid – From Evaporator Expansion Valve to Evaporator
4 - gas – From Evaporator to Absorber
5 - weak – From Absorber to Pump
6 - weak – From Pump to Solution Heat Exchanger (SHX) II
7 - weak – From SHX II to SHX I
8 - strong – From Generator II to SHX II
9 - strong – From Solution HX II to Absorber Expansion Valve
10 - strong – From Absorber Expansion Valve to Absorber
11 - weak – From SHX I to Generator I
12 - med – From Generator I to SHX I
13 - med – From SHX I to Expansion Valve
14 - med – From Expansion Valve to Generator II
15 - gas – From Generator I to Generator II
16 - liquid – From Generator II to Expansion Valve
17 - liquid – From Expansion Valve to Condenser

The variables used in following equations are described as follows:

$\dot{m}_n$ = mass flow rate of stream *n*
X_n = mole fraction of LiBr in stream *n*
dilute = the weak LiBr/water solution that leaves the Absorber for Generator
medium = the moderate LiBr/water solution from Generator I to Generator II
concentrated = the strong LiBr/water solution leaving Generator for the Absorber
refrigerant = the pure refrigerant that leaves the Generator and goes to Condenser
Q_y = Heat flux (kW) to/from component *y*
Generator = where heat is added to boil refrigerant out of weak absorbent
Condenser = where boiled refrigerant is condensed into liquid before evaporation
Evaporator = where refrigerant is evaporated at cooling load to remove heat
Absorber = where evaporated refrigerant is absorbed into concentrated absorbent
h_n = enthalpy per mass (kJ/kg) of stream *n*, which comes from the thermodynamic relations described below and is a function of mole fraction and temperature for solutions, and pressure and temperature for pure gaseous refrigerant.
T_n = Temperature of stream *n*
$C_{p,n}$ = constant-pressure heat capacity of stream *n* entering SHX

The inputs to the chiller model from the FCS model are FCS exhaust gas enthalpy measurements: mass flow, temperature, and specific heat. The chiller model assumes fixed temperatures for the evaporator (5 ºC – chilled water) and for the condenser and absorber (32 °C – cooling water). Generator I Solution Temperature is set between 90 °C and 160 °C and is a function of fuel cell exhaust temperature (T_{exh}). This relationship accounts for the physical limitations of the LiBr solution, and creates a threshold pinch point temperature.

$$\Delta T = T_{gen1} = T_{exh} - T_{gen2} \tag{12}$$

where T_{gen2} is determined by the relationship:

$$T_{gen2} = 0.136(T_{exh} - 320\ ℃) + 90\ ℃ \tag{13}$$

Equations for mass conservation:

$$\dot{m}_{dilute} = \dot{m}_{concentrated} + \dot{m}_{refrigerant} \text{ (Total)} \tag{14}$$

$$\dot{m}_{concentrated} X_{concentrated} = \dot{m}_{dilute} X_{dilute} \text{ (LiBr)} \tag{15}$$

Flow rates for solutions:

$$\dot{m}_{dilute} = \frac{X_{concentrated}}{X_{concentrated} - X_{dilute}} \dot{m}_{refrigerant} \tag{16}$$

$$\dot{m}_{concentrated} = \frac{X_{dilute}}{X_{concentrated} - X_{dilute}} \dot{m}_{refrigerant} \tag{17}$$

Circulation ratio is mass flow of concentrated solution to that of the refrigerant:

$$CR = \frac{\dot{m}_{concentrated}}{\dot{m}_{refrigerant}} \tag{18}$$

COP is a measure of the cooling load heat removed over the heat added (Note: Pump work would add to the denominator, but is omitted):

$$COP = \frac{Q_{evap}}{Q_{gen1} + Q_{gen2}} \tag{19}$$

There is an internal SHX that transfers heat from the hot concentrated solution leaving the generator to the warm dilute solution entering the generator from the absorber. The SHX effectiveness is defined as:

$$\psi_{SHX} = \frac{T_8 - T_9}{T_8 - T_6} \tag{20}$$

- ψ is zero (0) if no heat is transferred and the concentrated and dilute solutions exit at the same temperature they entered the SHX, and
- ψ is one (1) if all heat is transferred.

Assuming constant specific heat for streams across their inlet and outlet temperature range, solution temperatures are:

$$T_7 = T_6 + \frac{(h_8 - h_9)}{\dot{m}_7 C_{p,7}} \tag{21}$$

$$T_9 = T_8 - \psi_{SHE}(T_8 - T_6) \tag{22}$$

$$T_{11} = T_7 + \frac{(h_{12} - h_{13})}{\dot{m}_{11} C_{p,11}} \tag{23}$$

$$T_{13} = T_{12} - \psi_{SHX}(T_{12} - T_7) \tag{24}$$

When combined with the thermodynamic relations for enthalpy of mixtures at given temperatures, the equations above will output a COP for selected temperature values, concentrated and dilute solution concentrations, and SHX effectiveness. The temperatures are set by the heat source, the cooling tower parameters, and the cooling load.

The equations of the double-effect cycle are based on conservation of mass and energy and involve two SHXs (both of which are treated as similar in performance). The following equations result when energy and mass balances are performed:

$$Q_{Generator} = \dot{m}_{15} h_{15} + \dot{m}_{12} h_{12} - \dot{m}_{11} h_{11} \tag{25}$$

$$Q_{Condenser} = \dot{m}_2 h_2 - \dot{m}_1 h_1 - \dot{m}_{17} h_{17} \tag{26}$$

$$Q_{Evaporator} = \dot{m}_4 h_4 - \dot{m}_3 h_3 \tag{27}$$

$$Q_{Absorber} = \dot{m}_5 h_5 - \dot{m}_4 h_4 - \dot{m}_{10} h_{10} \tag{28}$$

A final assumption needs to be made in regards to the energy balance in Generator II. This is where the refrigerant from the first generator condenses and transfers its heat to the medium-concentration LiBr/water solution to boil off additional refrigerant. The incoming medium-concentration LiBr/water solution is typically hotter than the generator and contributes some of its heat to boiling off additional refrigerant too. This situation arises because the solution goes through an expansion valve; at the higher pressure refrigerant will not boil off, but at the lower pressure it does. The assumption made is that the enthalpy going in to Generator II equals the enthalpy coming out, and from this assumption the mass flow of refrigerant from Generator II can be calculated.

$$\dot{m}_1 = \frac{\dot{m}_{15} h_{15} + \dot{m}_{14} h_{14} - \dot{m}_{16} h_{16} - \dot{m}_8 h_8}{h_1} \tag{29}$$

2.4.3. Model Verification

The chiller model is verified by comparing its results against results from leading chiller models in the literature. Figure 9 displays the modeled relationship between the COP and the gas inlet temperature to Generator 1 compared to a model from literature [24]; the models show consistent agreement throughout most of the temperature range shown.

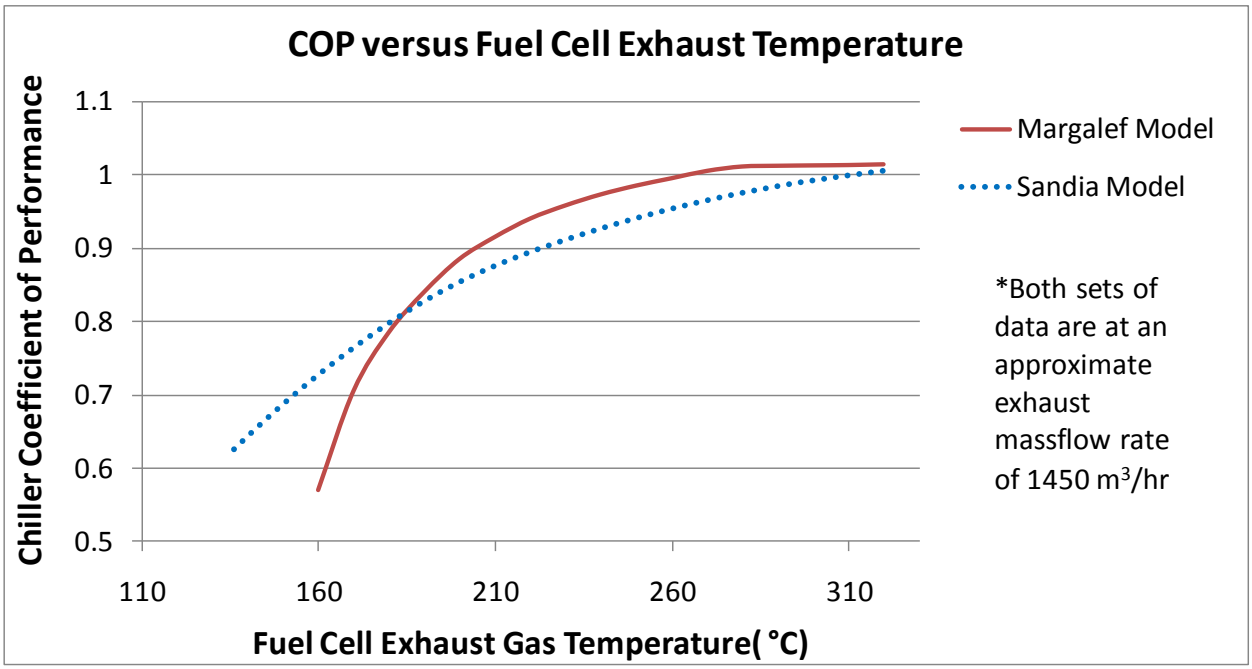

Figure 9. Model comparison of chiller COP versus fuel cell exhaust gas temperature.

The chiller model concurs with leading literature models in describing the relationship between chiller cooling output and gas inlet temperature as well as with manufacturers' data on the relationship between chiller cooling output and fuel cell exhaust flow rate. Figure 10 compares model output to that of Yazaki Energy Systems' absorption chiller [35]. The simulated chiller from the model is matched in both configuration and capacity to this commercial chiller.

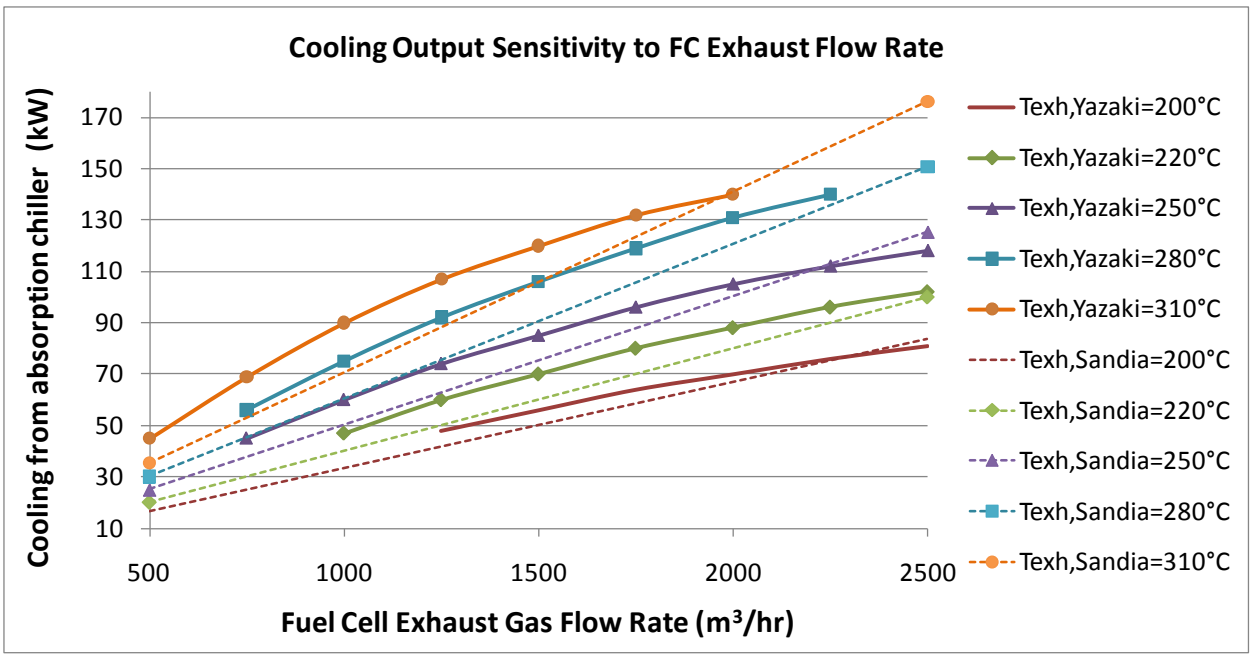

Figure 10. Comparison of model and equipment manufacturer's data for chiller output.

3. Results

3.1. Potential GHG Impact of Stationary FCSs

For the four fuel cell types and for the three numbered cases listed in Section 2.1, Table 4 shows the cumulative change in CO_2 emissions over the 15-year period in million metric tonnes (MMT). Fuel cells could either increase or decrease CO_2 emissions, depending on which types are installed and the type of electricity they replace.

Table 4. Changes in CO_2 Emissions With Fuel Cells Replacing California Power Plants.

Cumulative Change in CO_2 1990-2004 (MMT)				
Replace	**PEM**	**PAFC**	**MCFC**	**SOFC**
All Electricity Consumption	848	549	-54	-186
All In-State Generation	858	627	163	62
All Imports	-10	-78	-217	-247

For this scenario and the 1990-2004 period, three primary conclusions can be made:

1. All fuel cell types will reduce CO_2 if they replace imported electricity.
2. CO_2 emissions can be reduced the most if MCFC or SOFC systems replace imported electricity.
3. PEMFC and PAFC systems must be designed, installed, and operated to achieve a high in-use heat recovery efficiency if these systems are to reduce CO_2 emissions. If they produce electricity only, they cannot achieve substantial CO_2 reductions.

Under these assumptions, all FCSs perform better than California's historical imported electricity, which is largely based on coal power. Coal plants operate at relatively low efficiencies (~30%). Coal also has a much higher carbon content per unit energy (~29 kilograms of carbon/per kilojoule of fuel energy) than natural gas (~15.5 kilograms of carbon/per kilojoule of fuel energy). As a result, if fueled by natural gas, an FCS will produce some CO_2, but less than coal plants. If an FCS replaces imported generation into the state, it is replacing high carbon-emitting electric power with low carbon-emitting power. In summary, based on the assumptions above, the CO_2 emission factor (CO_2 per unit of electric power) for imported power is higher than the CO_2 emission factor for all fuel cell types.

Under the assumptions above, none of the FCSs perform better than California's collective in-state electrical power production. California's current in-state electrical production consists of mostly combined cycle natural gas turbines that achieve high electrical efficiencies (~50%) and non-carbon-emitting power plants such as nuclear, geothermal, hydroelectric, wind, and solar photovoltaic. If fueled by natural gas, an FCS will produce some CO_2. If an FCS replaces in-state generation, it is replacing some non-carbon-emitting electric power with carbon-emitting

power. In summary, based on the above assumptions, the CO_2 emission factor (CO_2 per unit of electric power) for the in-state grid is lower than the CO_2 emission factor for all fuel cell types.

There is some uncertainty in these estimates, especially as related to the actual performance of FCSs in the field and how quickly developers can move down learning curves. For example, learning curves affect how quickly systems can achieve high sustained average electrical efficiencies in operation. Developers can reduce uncertainties and move down these curves more quickly with more opportunities to install their systems.

These findings imply that FCSs should be designed to effectively recover useful heat through CHP if they are to reduce CO_2 emissions compared with low carbon emission generators and power grids.

3.2. Optimizing the Design of CHP FCSs

Model results are discussed for a case study example of a California town and generalized for a diverse audience. Model results show that the most optimal strategies for cost and CO_2 savings differ, but both invoke novel approaches. Model results indicate that energy cost savings and CO_2 reductions are highest with permutations that simultaneously invoke a combination of ―business-as-usual" and novel approaches. The strategy with the highest cost savings combines cogeneration, networking, VHP, NLF for the primary control at maximum electrical output, and subsequent heat load following for the secondary control. Results assume a base case with no FCSs installed and most power and heat provided by a cogenerative CCGT and any additional electricity supplied by the average mix of power plants in California.

Cost optima are most sensitive to (1) the FCS maximum electrical output, (2) the FCS electrical efficiency, and (3) the natural gas, steam, and electricity prices. CO_2 optima are most sensitive to (1) FCS electrical efficiency, (2) the maximum heat-to-power ratio, and (3) FCS heat recovery efficiency. For the strategies optimized for cost or CO_2, the electrical and thermal capacity utilizations of the FCSs approach 100%. Optimal strategies differ for cost savings and profit. Strategy 12 [NVEXH] is novel and results in the most cost savings. The resulting installation has excess thermal capacity and a larger number of units than needed for heat demand. Strategy 6 [NFEXHN] is a more conventional, ―plain vanilla" approach but leads to the greatest revenue, sales, and profit for FCS manufacturers. (Example results discussed here are for scenario D: full state and federal incentives, and a \$100/$MTCO_2$ carbon tax.)

Likewise, optimal strategies differ for cost and CO_2 savings. Strategy 12 [NVEXH] is novel and has the most cost savings while Strategy 11 [NVHEX] is novel and has the most CO_2 reduction. This is shown below in Figure 11.

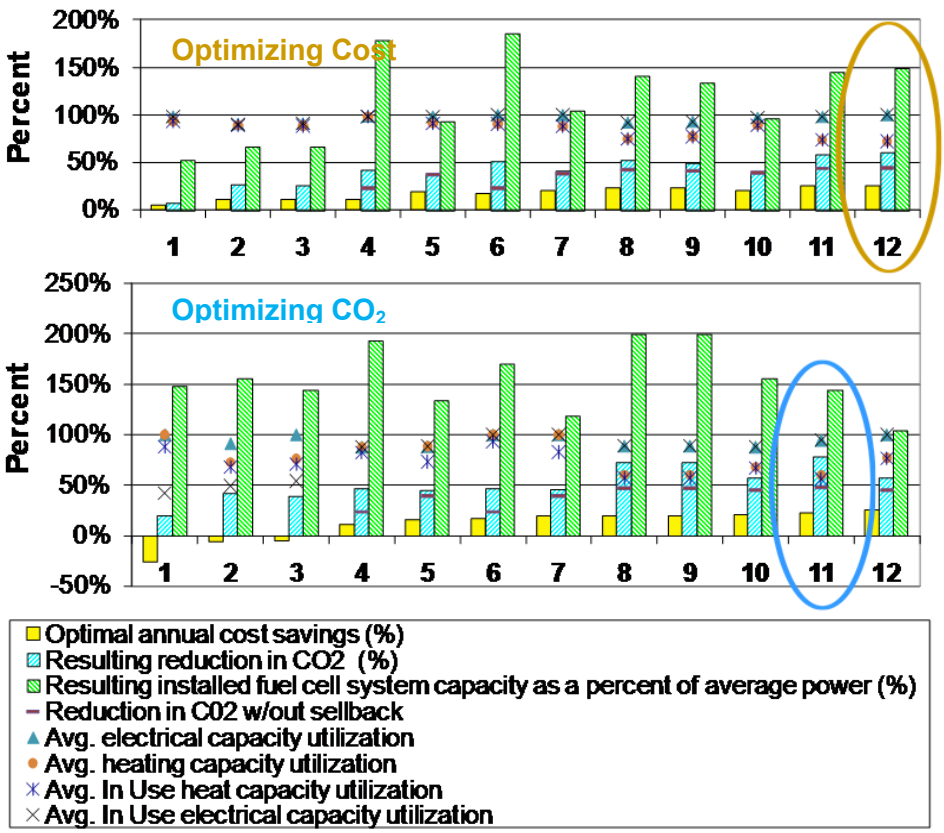

Figure 11. Cost optimization vs. CO_2 optimization.

In most cases, when optimized for cost, networked (N) strategies (4 to 12) show higher cost savings than stand-alone (S) strategies (1 to 3). The advantage in cost savings for networked strategies is shown clearly below in Figure 12. Figure 12 compares identical FCS strategies, except that one configuration is networked while the other is stand-alone. Strategies 1 and 6 are an identical pair, except that Strategy 1 is stand-alone while Strategy 6 is networked. Similarly, Strategies 2 and 9 are also an identical pair of stand-alone and networked strategies, respectively. So are Strategies 3 and 12. In each case the networked case outperforms the stand-alone case in cost savings, CO_2 emission reductions, and manufacturer profit. Networked systems can be installed in larger numbers than stand-alone systems, while maintaining or increasing energy cost savings to building owners.

Strategies 9 and 12 have lower heat capacity utilizations when compared to their stand-alone counterparts, Strategies 2 and 3. The networked buildings are able to sell electricity back to the grid for revenue, such that there is less of a penalty associated with installing a larger FCS capacity because the excess electricity is not being wasted but instead sold back to the grid for revenue. This increased FCS capacity results in additional heat energy capacity available that is used a lower portion of the time for the networked strategies compared with stand-alone ones.

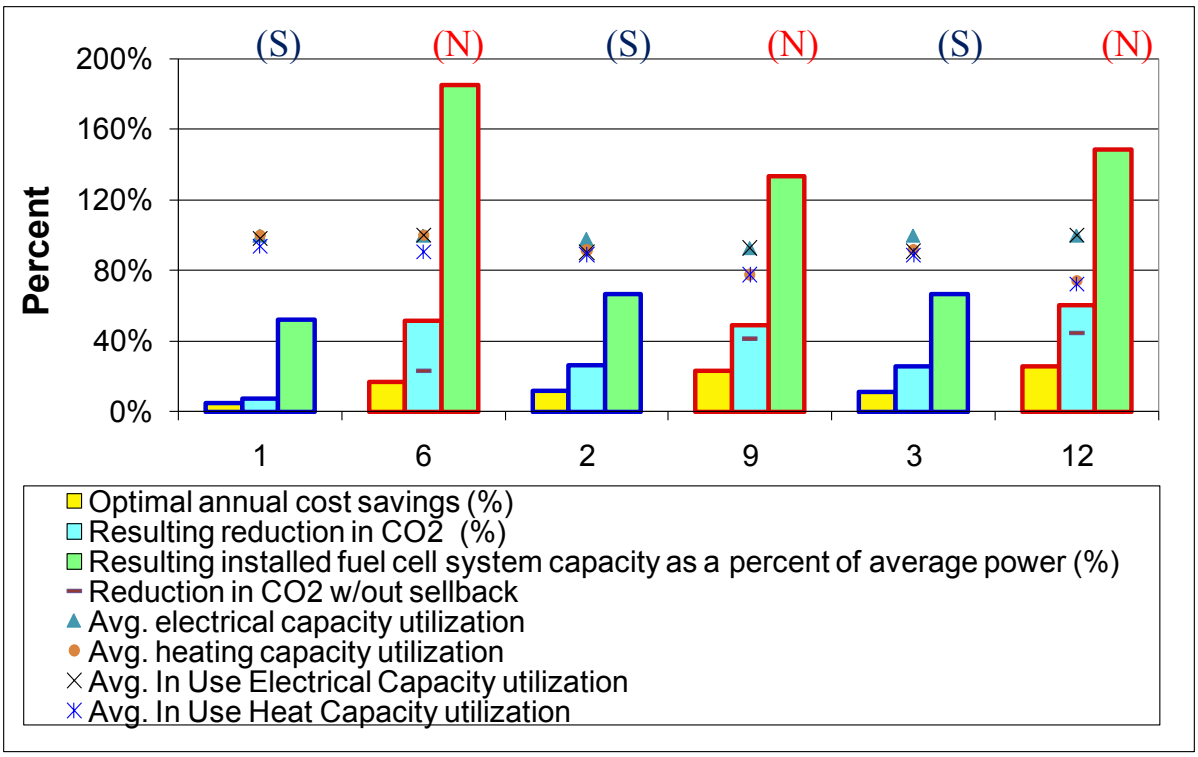

Figure 12. Cost optimization, same configuration for networked vs. stand-alone.

Optimal cost savings for networked installations is always larger than for stand-alone installations, and this optimal point always occurs at a larger installed capacity for networked systems compared with stand-alone ones. For networked installations, optimal cost savings occurs at an operating point consistent with covering a very large portion of the thermal demand distribution. For stand-alone installations, optimal cost savings occurs at an operating point consistent with covering a large portion of both the limited thermal and electrical demand. For stand-alone installations, optimal savings occur at a lower installed capacity, where less of the energy produced is wasted. With stand-alone installations, at higher installation levels, a greater portion of the energy produced is lost because the heat and electricity cannot be distributed to other buildings or to the grid (unlike with networking).

Figure 13 shows cost savings for both networked and stand-alone approaches as a function of the heat that they supply and their installed capacity. The networked strategy shown is Strategy 9 and the stand-alone strategy is Strategy 2 (a matching pair). In Figure 13, "heat demand" (represented by a single grey bar) is the number of hours in a year that heat is needed by buildings in an energy area within a certain heat demand range that is organized into 500-kilowatt segments. "Heat demand distribution" (the distribution of all of the grey bars combined) is the histogram of heat demand from all buildings in an energy area over one year. "Installed capacity" is a non-dimensional term proportional to the number of FCSs installed and in operation; it can be described as the maximum electrical output of all installed FCSs divided by the average electrical demand from that energy area. "Cost savings" is the money building owners save on electricity and heat costs when they switch from a base case generator to FCSs,

as a percentage of their base case expenditure. (To make results more applicable to a broader audience, data units are non-dimensionalized wherever possible.)

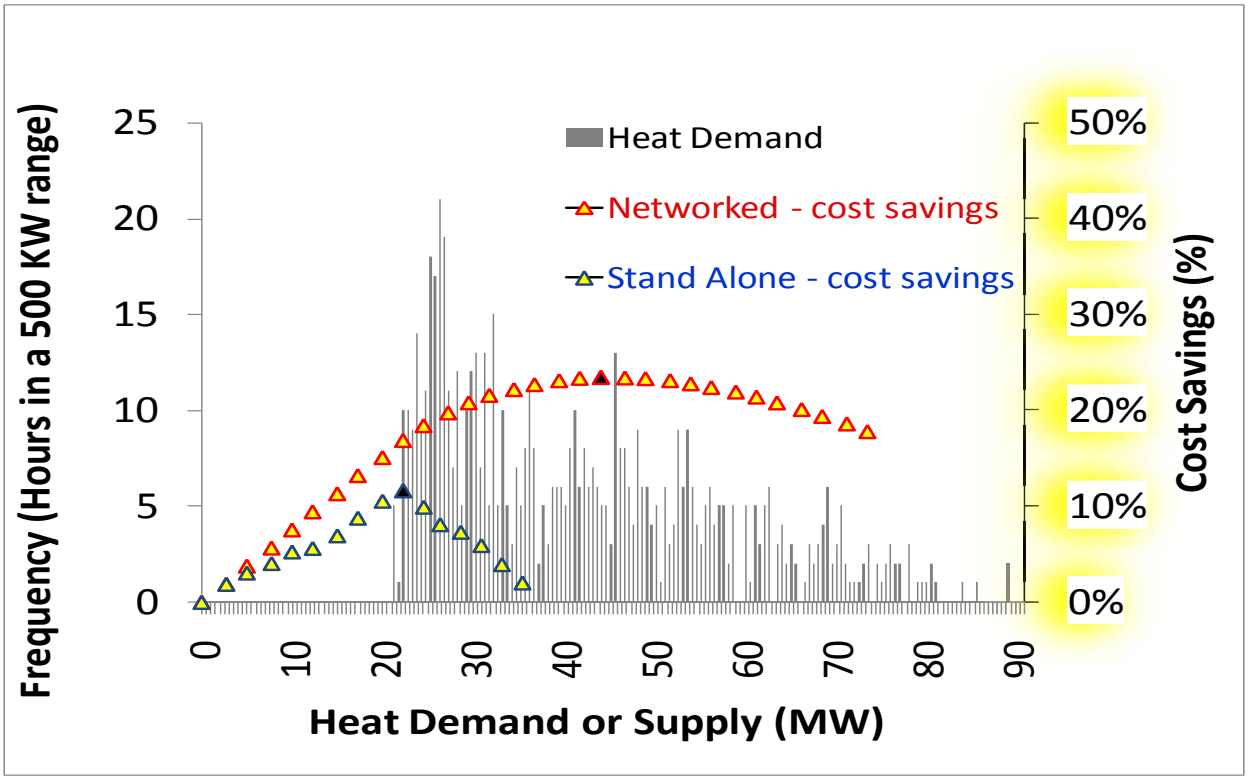

Figure 13. Histogram of heat demand and supply vs. cost savings for networked and stand-alone FCSs.

For the networked strategy, the cost optimum occurs at an installed capacity of 133% (shown in the figure by the blackened triangle). At this point, heat supplied by the FCS meets a very large segment of the thermal demand distribution (shown in grey). For cost optima for network strategies, the optimal installed capacity is largely a function of the portion of the thermal demand distribution being met. The optimal point occurs where a large segment of the thermal demand is met by the FCS.

For the stand-alone strategy, the cost optimum occurs at an installed capacity of only 52% (shown in the figure by the blackened triangle). At this point, heat supplied by the FCS meets only a portion of the thermal demand distribution (shown in grey). For cost optima for stand-alone strategies, the optimal installed capacity is a function of the portions of both the electrical and the thermal demand distributions being met. The optimal point occurs where a portion of both the local electrical and thermal demand is met by the FCS. Since stand-alone systems cannot sell electricity back to the grid, the size of the effective electrical demand distribution is smaller, and requires fewer FCSs to serve it. For either networked or stand-alone strategies, as the number of installations increases beyond the optimal point for each, the quantity of wasted energy increases and the cost savings declines.

3.3. Optimizing the Design of CCHP FCSs

Computer simulations with CCHP FCS models demonstrate a few salient results that can be generalized for different cases. First, for most of the permutations investigated, Strategy vii [EX, H, C] is the most economical. However, for some permutations, either Strategy v [E, H, C] or viii [EX, C, H] is most economical, usually when there is no grid connection. Second, thermal storage is occasionally economical while cooling storage is rarely economical and electrical storage is never economical. Finally, for the permutations investigated, Strategies v [E, H, C] and vii [EX, H, C] have the lowest CO_2 emissions. Please see Figure 14.

Costs are lowest with Strategy vii [EX, H, C], ie. the approach of networking; VHP; tunable cooling-to-heat; maximum electrical as the primary control; and load following heat and then cooling demands. As long as systems are grid-connected with a competitive electricity sell-back price, they can sell excess electricity not used in the local area for revenue. By contrast, both heat and cooling demands are locally constrained, without storage.

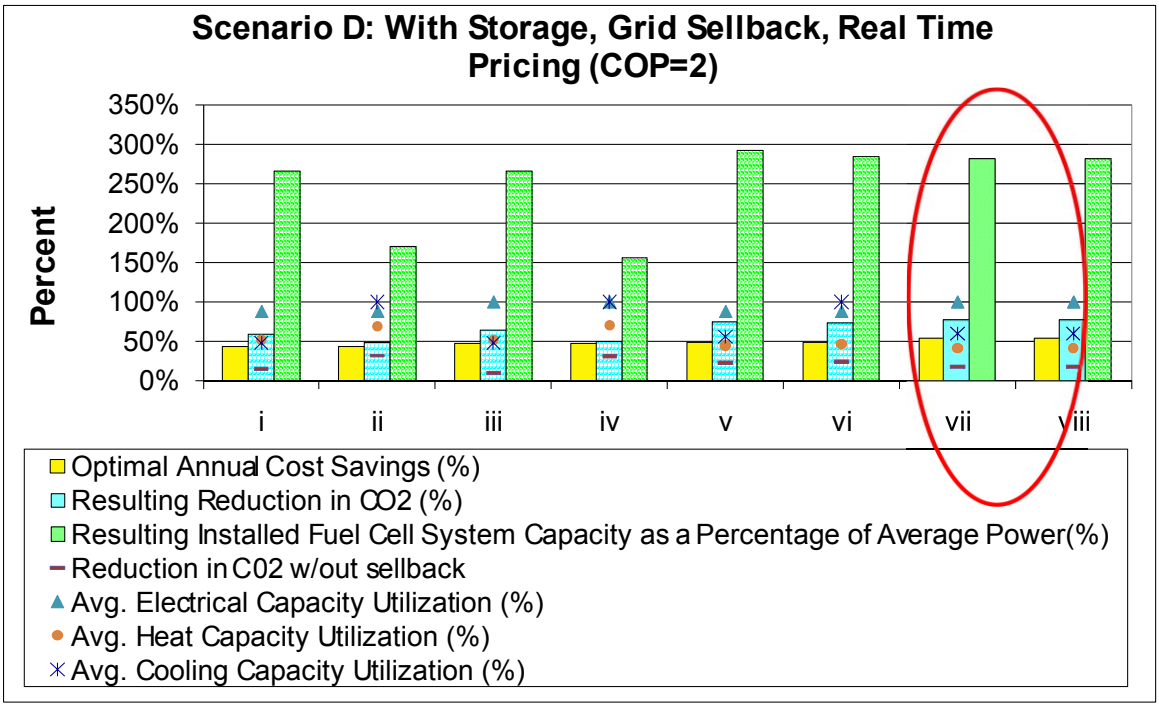

Figure 14. Cost optimization, Scenario D, COP = 2.

- Figure 14 shows that strategy vii with a COP of 2 experiences the largest cost savings.
- With a large COP, FCS tends to experience more similar cost savings among strategies because of their ability to produce a larger portion of the cooling demand.
- The heat capacity utilization is generally 50% or below for all strategies except strategies ii and iv, which are both configured as HX (maximum heat) as the tertiary control. Instead of producing recoverable heat, it is more economical for CCHP FCSs with COPs of 2 to produce a greater portion of cooling power.

An additional finding is that the optimal strategy for cost minimization changes with the relative price of cooling to heating. As the competing generator cooling price changes, the optimal order changes for primary, secondary, and tertiary control of (1) maximum electrical output, (2) heat load following, and (3) cooling load following. For example, as the cooling price increases to four times its standard value, the most economical strategy changes from NVYEXHC with cooling load following as the tertiary control to NVYEXCH with cooling load following as the secondary control. This point is illustrated in Figure 15.

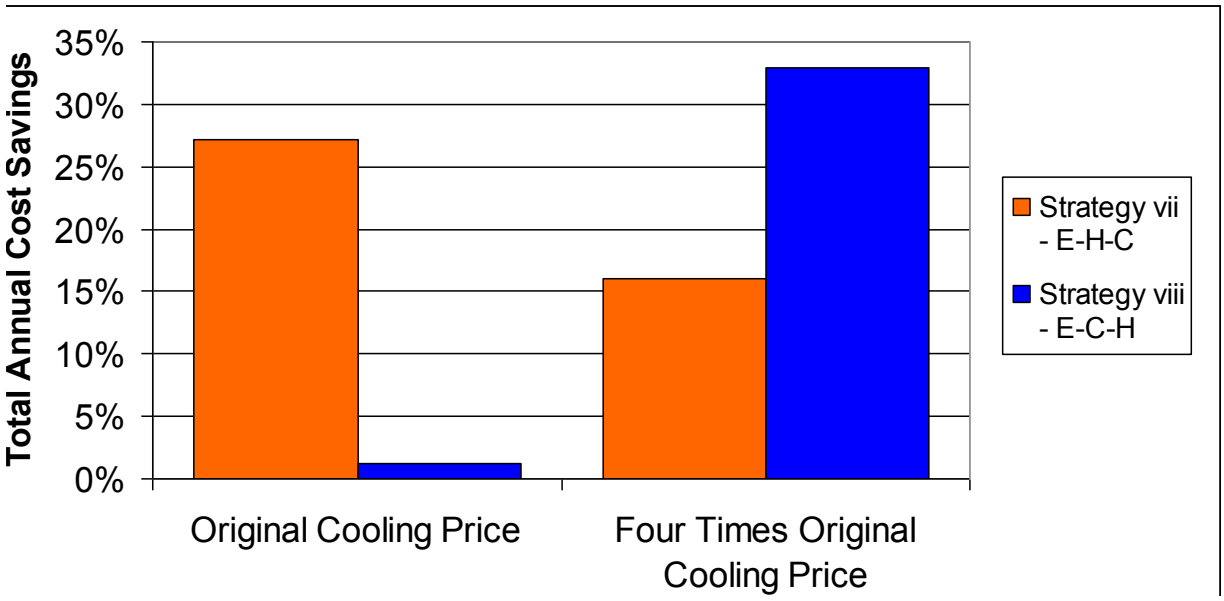

Figure 15. Optimal strategy changes with energy cost.

Strategy viii shows bimodal optimal heating storage capacity when optimizing for cost, which is caused by the seasonal shape of the demand curve and is shown in Figure 16.

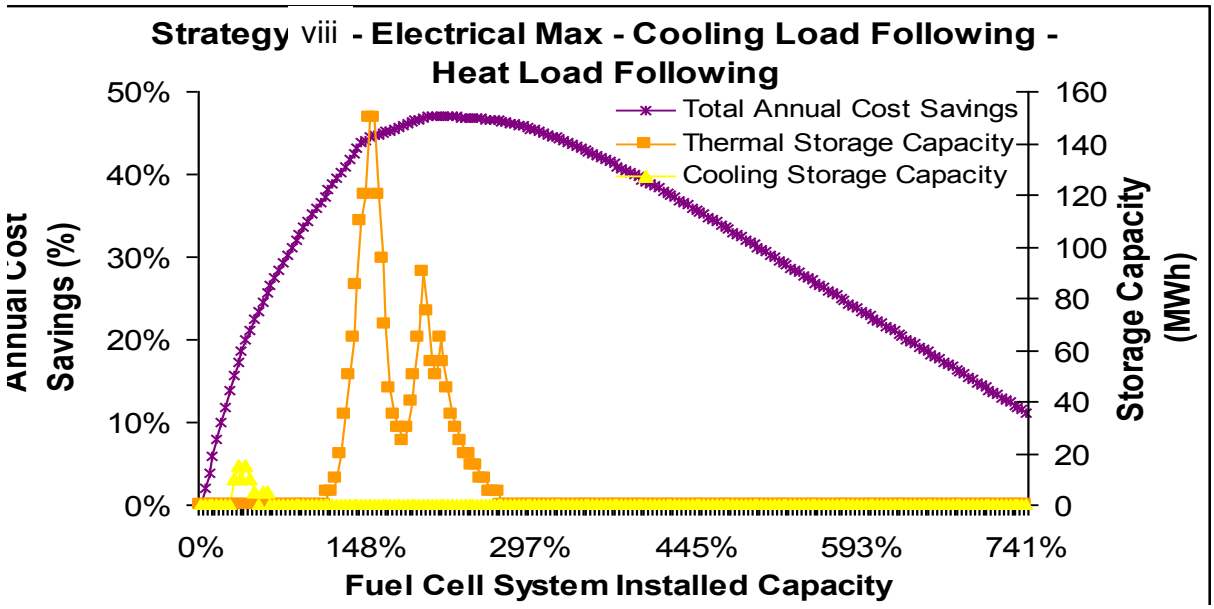

Figure 16. Cost savings and thermal storage capacity.

The cost optimal strategy can also change with the COP. Figure 17 shows the relative cost savings for Strategies v, vii, and viii with COPs of 0.5, 1, and 2, respectively. Without grid

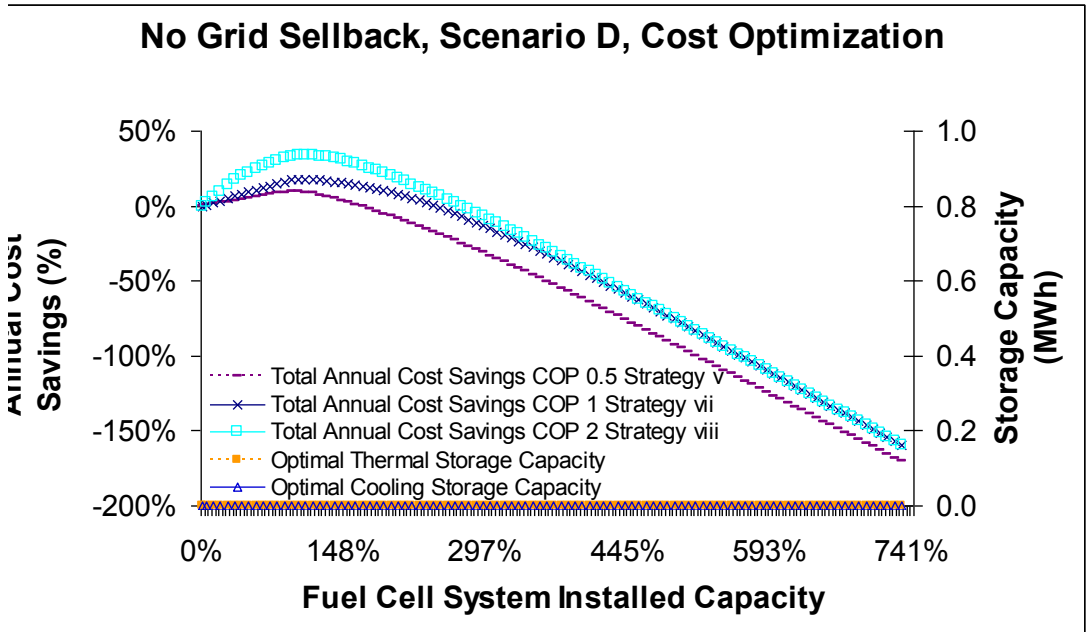

Figure 17. Cost savings comparison for COP = 0.5 to 2.0.

sellback, at COP = 0.5, Strategy v is most cost-effective. At COP = 1 and 2, Strategies vii and viii are most cost-effective, respectively. The cost savings becomes negative after a certain installed capacity for each strategy. Strategies vii and viii begin to mirror each other after a certain installed capacity because all of the cooling energy is being met. Regardless of whether cooling loading following is a secondary or tertiary control, once the installed capacity reaches a certain value, all thermal and cooling energy demand will be met regardless of the difference in COP.

In general, CO_2 emissions are lowest with strategies that use electrical, thermal, and cooling networking; VHP; tunable output of total cooling to recoverable heat; and either maximum electrical output or load following electricity, and then load following heat and cooling demands. Less fuel is wasted.

At low COP, the CO_2 minimizing strategy is vii – EX, H, C. At higher COP, the CO_2 minimizing strategy is v – E, H, C. The order of load following constraints that most benefits CO_2 is EX/E, H, C. At higher COP, Strategy v is more effective than Strategy vii because load following electricity consumes less fuel. At a low COP, the additional electrical output from having electrical production fixed at a maximum for the primary control outweighs the effects of additional fuel consumption because of the additional thermal and cooling demand that is able to be met. However, as the COP increases, for CO_2 minimization, it is most beneficial to load follow electricity to conserve fuel.

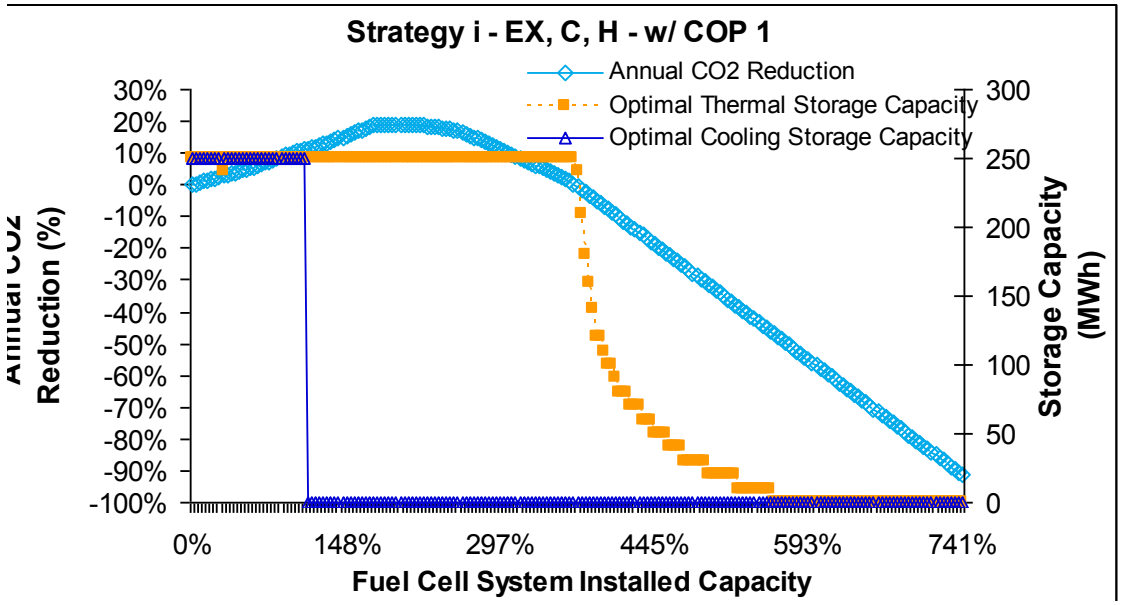

Figure 18. CO_2 optimization, Strategy I, COP = 1.

Figure 18 shows example results for CO_2 optimization. This analysis assumes that the cooling storage capacity begins full and that there is no associated CO_2 penalty with the initial cooling energy stored. An important point that this figure illustrates is that it becomes a detriment rather than a benefit to run the FCS at a higher VHP to refill the cooling storage capacity. The additional fuel that the FCS consumes by running at a higher VHP does not allow it to outperform competing generators who are producing cooling energy with a lower carbon footprint. (This result contrasts previous results for CHP FCS, which show benefits from the use of a higher FCS VHP to recharge the thermal storage capacity.)

Previous studies showed only a benefit to a VHP for reducing CO_2 with CHP FCSs (not CCHP FCSs). Results showed that largest gain in CO_2 reductions occurs with the initial increase in VHP. As VHP meets a greater percentage of heat demand, there are diminishing returns to increasing the VHP range further.

3.4. Thermodynamic and Chemical Engineering Models of CCHP

For our integrated thermodynamic and chemical engineering model, example results are shown for CCHP FCS performance for the following key input variables and parameters:

- Fuel – Methane (CH_4)
- Oxidant – Air
- Steam-to-Carbon Ratio (molar basis) = 3
- Fuel Cell Operating Temperature = 750 °C
- Anode fuel utilization = 50–90%
- Cathode oxygen utilization = 15–28%
- Fuel Cell current density = 200–800 milli-Amps per centimeter squared (mA/cm^2)

- Air-to-Fuel Ratio (molar basis) = 17–30
- Chiller inlet temperature is constant at the generator = 350 °C
  - Controlled by air addition
- Chiller inlet mole flow is variable
- Heat recovery after chiller assumed to exhaust at 25 °C

An important result is that fuel cell operating conditions such as fuel utilization and current density have a strong impact on CCHP efficiencies, which include electrical (ϵ_{elec}), heat (ϵ_{heat}), and cooling ($\epsilon_{cooling}$) efficiencies. These efficiencies can be defined as follows:

$$\epsilon_{elec} = \frac{P_{gross\ elec} - P_{parasitic}}{\Delta H_{rxn}} \tag{30}$$

$$\epsilon_{heat} = \frac{Q_{recoverable}}{\Delta H_{rxn}} \tag{31}$$

$$\epsilon_{cooling} = \frac{Q_{Evaporator}}{\Delta H_{rxn}} \tag{32}$$

In the equations above, $P_{grosselec}$ is the gross electrical power output of the fuel cell stack. $P_{parasitic}$ is the sum of electrical parasitic loads associated with gas compression and liquid pumping. ΔH_{rxn} is the change in enthalpy for the combustion reaction of the inlet fuel at standard temperature and pressure (STP) with liquid water products, or the inlet fuel's energy content based on the higher heating value (HHV). $Q_{recoverable}$ is the heat available after the absorption cycle that could be used for low-temperature heating applications such as hot water and space heating. $Q_{Evaporator}$ is the cooling power available from the absorption cycle.

Example model results for these efficiencies are shown in Figure 19. The figure shows these efficiencies as a function of the fuel inlet flow rate. These results are for an SOFC system operating at these datum design conditions: 200 mA/cm^2, fuel utilization of 85%, oxygen utilization of 28%. As shown, when electrical efficiency peaks, the cooling efficiency exhibits a minimum. The reason for this effect is that, when the fuel cell operates at its maximum electrical efficiency, the total quantity of unused heat (for either heat recovery or cooling power) is at a minimum. As the electrical efficiency decreases, the cooling efficiency increases because more unused heat is available to the absorption chiller for generating cooling power. For this particular approach to absorption chiller integration, the heat efficiency decreases as the fuel inlet flow rate increases.

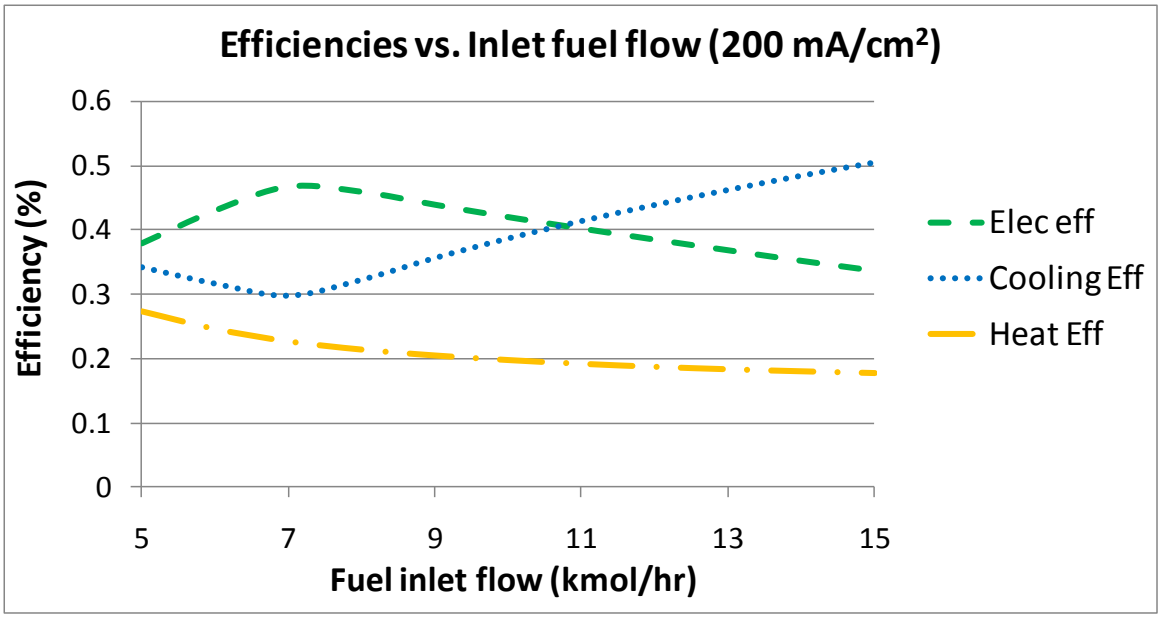

Figure 19. Efficiency versus fuel inlet flow at current density = 200 mA/cm^2.

Similar performance can be observed at higher current densities. Figure 20 plots similar results to Figure 19 but at a current density of 400 mA/cm^2; fuel and oxygen utilization remain constant at 85% and 28%, respectively. At higher current densities, with all other operating conditions held constant, voltage losses (polarizations) are greater. More unused heat is available. As a result, at higher current densities, the net electrical efficiency is lower while the combination of the recoverable heat and the cooling power can be expected to be higher. This trend can be seen in comparing the figures.

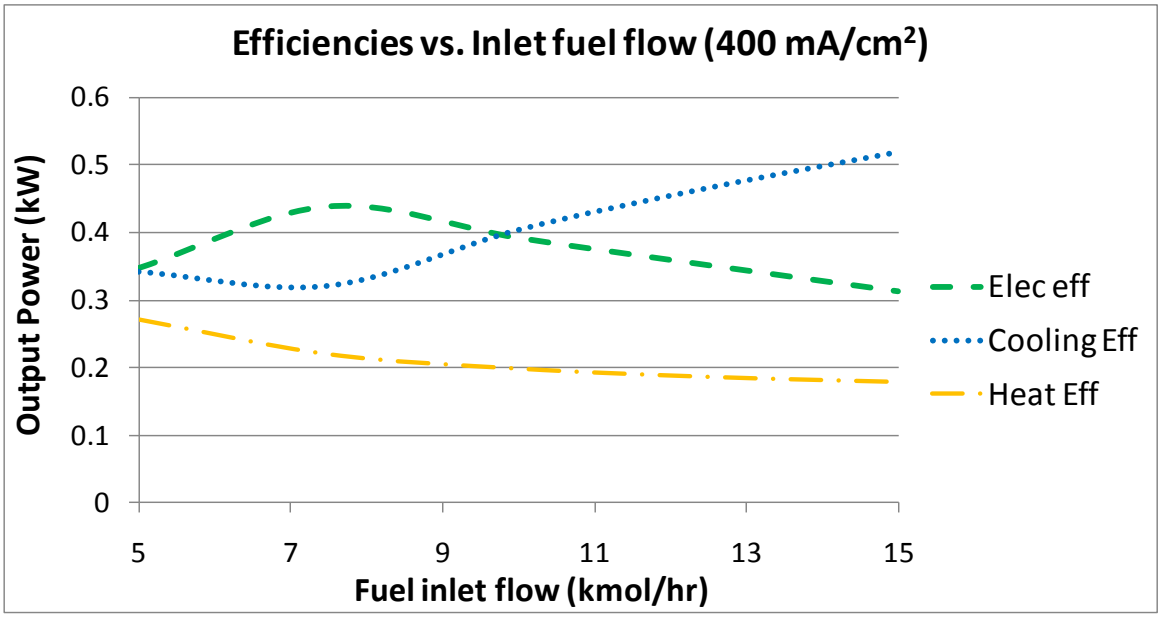

Figure 20. Efficiency versus fuel inlet flow at current density = 400 mA/cm^2.

Example model results for these efficiencies are shown also as a function of fuel utilization. As shown in Figure 21, electrical efficiency increases as the fuel utilization increases, reaching values higher than 50% at utilization factors of 90%. A typical fuel cell utilization factor is 85%. As shown in Figure 21, cooling efficiency decreases as the fuel utilization increases. Cooling efficiency decreases as the fuel utilization increases because the total quantity of unused heat available declines as the SOFC system becomes more electrically efficient. The sum of the cooling and heat recovery efficiencies follows the inverse pattern of the electrical efficiency, due to the principle of conservation of energy.

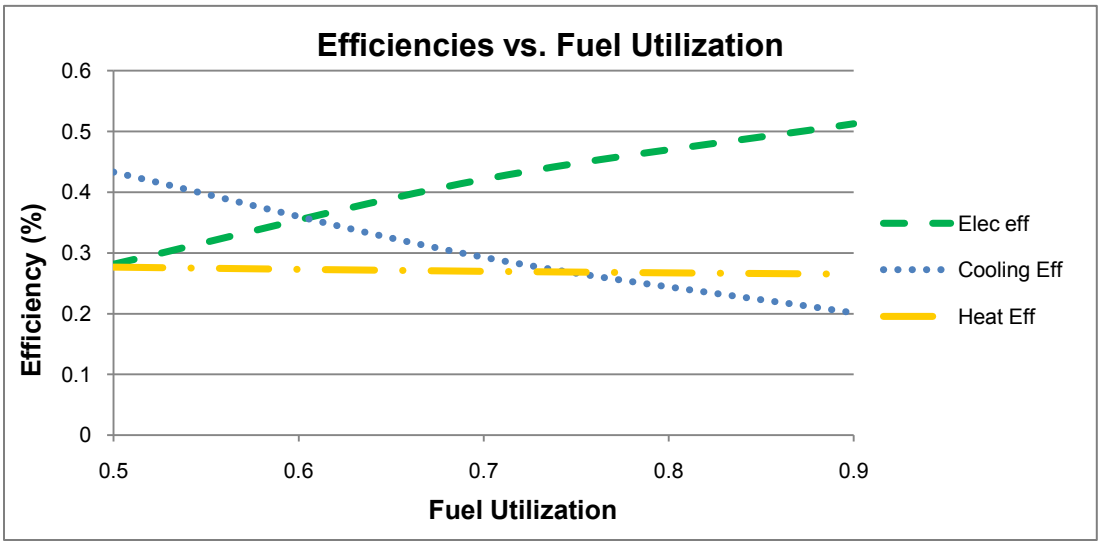

Figure 21. Efficiency versus fuel utilization.

Example model results also plot different types of energy outputs as a function of fuel utilization. As a function of fuel utilization, Figure 22 plots fuel energy input, gross electric power output, cooling power output, recoverable heat, and parasitic power, at a constant 200 mA/cm^2. As fuel utilization increases, the gross electric power output increases and the cooling power decreases, for similar reasons as discussed above. Heat input (Q_{in}) and $Q_{parasitic}$ remain constant.

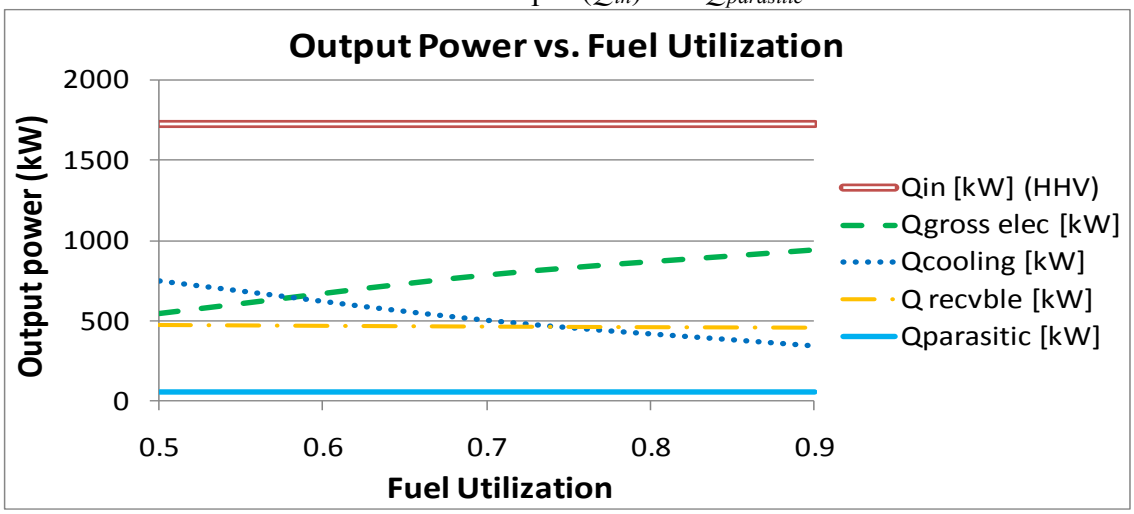

Figure 22. Output power versus fuel utilization.

Model results also plot different types of energy outputs as a function of fuel inlet flow rate. Figure 23 shows the relationship between output power and fuel inlet flow rate at 200 mA/cm^2. Total power output from gross electricity, cooling, and recoverable heat increase with flow rate. By contrast, parasitic power remains fairly constant. At a higher current densities, polarization losses are greater, such that the electrical efficiency peaks at a lower value, and more combined cooling and heating are available. The overall patterns remain the same.

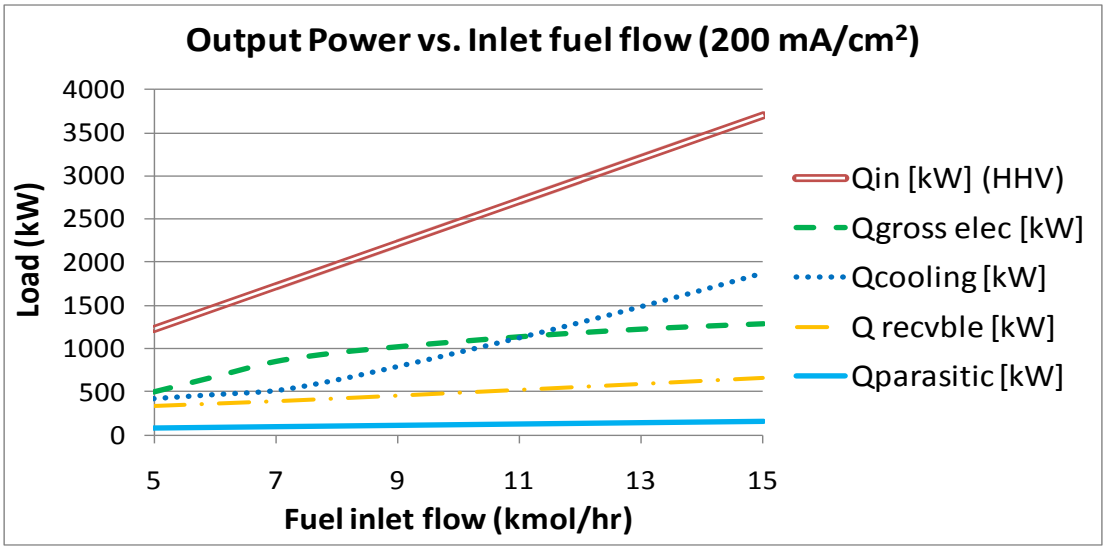

Figure 23. Individual system outputs versus inlet fuel flow.

Model results also can compare overall efficiency for CHP and CCHP FCSs. Figure 24 plots system efficiencies versus fuel flow for both. Datum design conditions are 85% fuel utilization, 28% oxygen utilization, and 200 mA/cm^2. CHP efficiency includes electrical and heat recovery efficiencies. CCHP includes electrical, heat recovery, and cooling efficiencies. Since the absorption chiller operates with a COP of slightly over 1, cooling performance is slight higher than heating performance, creating the effect shown below.

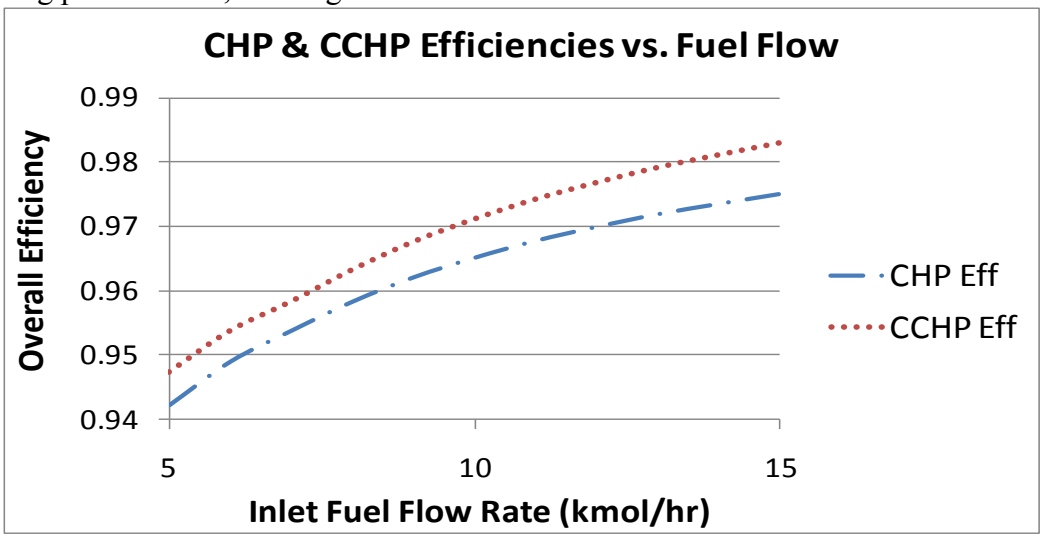

Figure 24. CHP and CCHP efficiencies versus fuel flow with a current density of 200mA/cm^2.

4. Conclusions

4.1. Potential GHG Impact of Stationary FCSs

For this scenario and the 1990-2004 period, three primary conclusions can be made regarding introducing stationary fuel cell systems into California:

1. All fuel cell types reduce CO_2 if they replace imported electricity.
2. CO_2 emissions can be reduced the most if MCFC or SOFC systems replace imported electricity into the state.
3. PEMFC and PAFC systems must be designed, installed, and operated to achieve a high effective heat recovery if these systems are to reduce CO_2 emissions. If they produce electricity only, they cannot achieve substantial CO_2 reductions.

Figure 25 shows estimated CO_2 emission changes for California using FCSs.

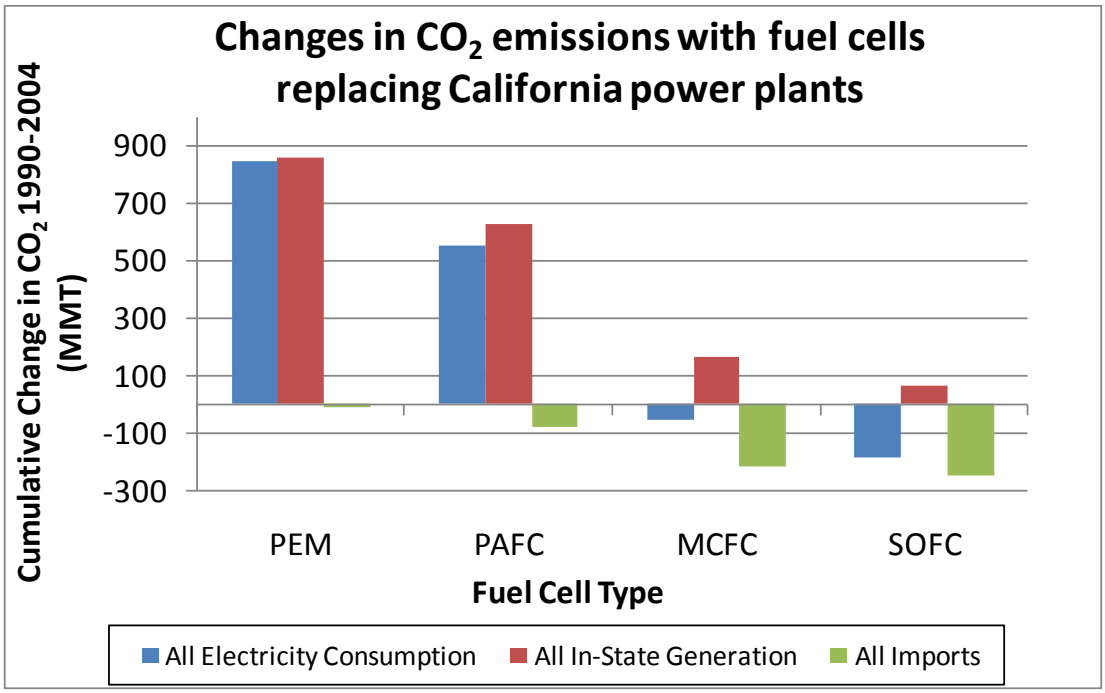

Figure 25. CO_2 emission changes for California using fuel cell systems.

Results indicate that FCSs should be designed to effectively recover heat through CHP if they are to reduce CO_2 emissions, compared with other low carbon generators and power grids. If PEMFC and PAFC are to reduce CO_2 effectively in California, they must be operated cogeneratively with high effective heat recovery. It has been shown that without highly effective heat recovery, their implementation could actually increase CO_2 emissions in California relative to the California mix of electric power.

4.2. Optimizing the Design of CHP FCSs

CHP FCS model results indicate important conclusions. Model results indicate that energy cost savings and CO_2 reductions are highest with permutations that simultaneously invoke a combination of "business-as-usual" and novel strategies. Energy costs and CO_2 emissions can be reduced significantly by switching from certain "business-as-usual" approaches to novel ones in the way that stationary FCSs are designed, controlled, installed, and operated.

CHP FCS model results indicate significant benefits to networking. For the same configuration, when optimized for cost, networked FCSs have a higher cost savings than stand-alone systems, as shown in Figure 26. Networked systems can also install a larger number of units while maintaining a high FCS capacity factor. Likewise, for the same configuration, when optimized for CO_2 reduction, networked systems have higher CO_2 savings than stand-alone systems. The CO_2 difference between networked and stand-alone systems is the displaced CO_2 from selling electricity back to the grid. Ignoring this, networked systems achieve the same CO_2 reduction as stand-alone systems but at much lower cost.

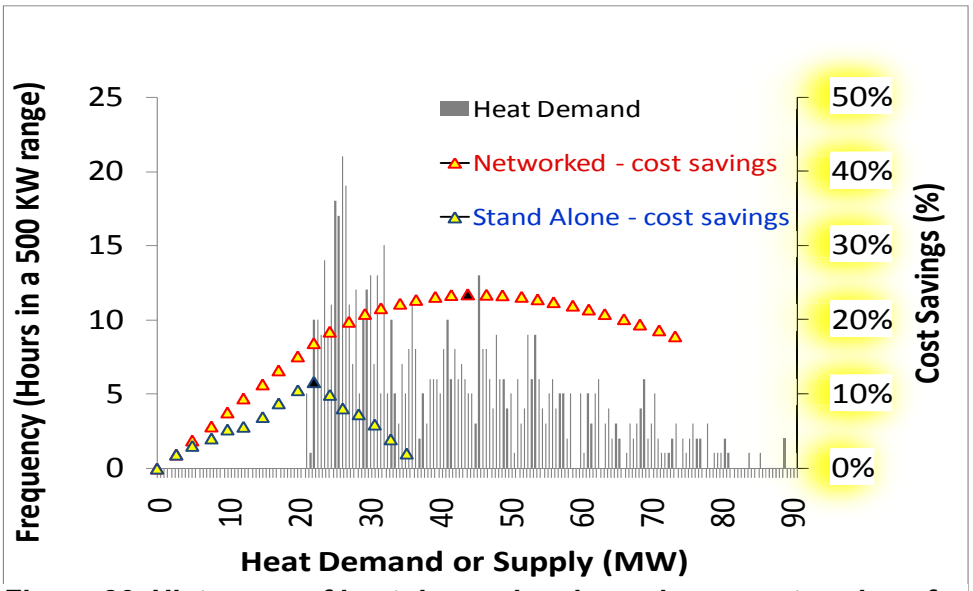

Figure 26. Histogram of heat demand and supply vs. cost savings for networked and stand-alone FCSs.

CHP FCS model results also indicate significant benefits to a VHP. An FCS employing a VHP results in higher energy cost savings than an FCS using an FHP above a certain maximum VHP. The largest gain in CO_2 emission reduction and cost savings comes with the initial increase in VHP. There are diminishing returns to increasing the VHP further as the VHP meets a larger percent of heat demand.

For the economic and engineering environments evaluated, CHP FCS model results indicate further conclusions relevant to diverse audiences. Models indicate that no one operating strategy achieves all economic and environmental goals under all scenarios. Different strategies achieve the diverse goals of cost savings to building owners, high fuel cell manufacturer sales, and CO_2 emission reductions. The environment sees the highest CO_2 reductions and building owners get

the highest energy cost savings by switching to strategies that invoke novel approaches. This beneficial switch includes changing from stand-alone (S) to network (N) followed by going from fixed (F) heat-to-power ratio to variable (V). Changing to novel strategies can improve energy cost savings and installed capacity as much as or more than increasing a carbon tax. The environment sees higher CO_2 reductions and building owners get higher energy cost savings by combining a carbon tax with certain novel approaches. For stand-alone FCSs, financial savings are maximized by installing FCSs in buildings with high constant demand for electricity and heat over time. Such buildings may include dry laboratories, wet laboratories, and 24-hour industrial facilities. For the California town examined here, relative to a base case of no FCSs installed, energy system optimization models indicate that novel operating strategies for CHP FCSs could reduce building energy costs by 25% and CO_2 emissions by 80%.

Model results support the importance of further research in these areas:

- Enhance the ability of an FCS to operate with a VHP. One approach for doing this is to develop the ability to operate a single fuel processing subsystem as an endothermic steam reformer, an exothermic partial oxidation unit, an autothermal reformer, or any combination of these to change the net heat released. This approach could be accomplished, for example, by altering the fuel processor's steam-to-carbon ratio. Another approach is to expand the operating range of the anode off-gas burner.
- Develop FCSs that are more durable under rapid changes in electrical and thermal load. One approach for doing this is to couple fuel cells with a variety of energy storage devices. Another approach is to develop cell materials and designs to increase cell durability under rapid cycling.
- Further develop and apply simulations of complex energy systems using technical-economic models [36].
- Continue to model the predilections of users and manufacturers, as well as positive impacts to the environment, and test methods for aligning them.

4.3. Optimizing the Design of CCHP FCSs

For the economic and engineering environments under consideration, several important conclusions can be drawn from CCHP FCS computer simulations. A key result is that global CO_2 emissions from cooling, electricity, and heat are lowest when CCHP FCSs are networked, use a VHP, use a tunable output of total cooling to recoverable heat, use a variable heat-to-power ratio, and load follow electricity, heat, and cooling demands as the primary, secondary, and tertiary controls, respectively. Less fuel is wasted with load following. A second key result is that global energy costs from cooling, electricity, and heat are lowest when CCHP FCSs are networked, use a tunable output of total cooling to recoverable heat, use a variable heat-to-power ratio, produce maximum electrical power continuously as the primary control and load follow heat and cooling demands as secondary and tertiary controls. As long as systems are grid-connected with a competitive electricity sell-back price, they can sell excess electricity not used in the local area for revenue. By contrast, both heat and cooling demands are locally constrained, either with storage (due to its high costs) or without storage.

For the scenarios evaluated, CCHP FCS simulations indicate additional important conclusions relevant to a broad audience. CCHP FCS model results indicate that the cost optimal strategy can change with several different parameters: the ratio of cooling price to heating price, the absorption chiller's COP, the electricity sellback price, and the ability to sellback to the regional electricity grid. For example, as the competing generator cooling price increases, it becomes more important to operate fuel cells in cooling load following mode rather than heat load following mode. For the engineering and market conditions investigated, models indicate that electricity storage is never economical at the optimal FCS installed capacity, cooling storage is rarely economical at the optimal FCS installed capacity, and thermal storage is, by contrast, sometimes cost-effective at the optimal installed FCS capacity. These results stem from the unit costs of these storage options. When optimizing for cost, optimal storage capacities can exhibit single modal, bi-modal, or multi-modal behavior. This modality results from a combination of the seasonal shape of the demand curves and the FCS operating parameters.

4.4. Thermodynamic and Chemical Engineering Models of CCHP

Chemical engineering models accurately describe the performance of high-temperature FCSs coupled with ACCs. Models couple double-effect lithium bromide (LiBr) ACC submodels with detailed SOFC system submodels. Submodels are verified against data from the literature and industry. Models reveal the expected performance for thermally integrated CCHP FCSs. This performance includes efficiency (electrical, heat, and cooling) and cooling power output as a function of fuel flow rate, fuel utilization, operating temperature, current density, and a variety of other operating conditions.

Chemical engineering models of CCHP FCS underscore a few salient conclusions. When electrical efficiency peaks, the combination of the heat recovery and cooling efficiencies exhibits a minimum. Cooling efficiency increases with changes in a few key parameters: as fuel flow rate increases beyond the peak electrical efficiency point; as stack electrical efficiency decreases; as stack current density increases; and as stack fuel utilization decreases. The reason for the increase in cooling efficiency with changes in these parameters is that these changes result in an increase in stack polarization and therefore an increase in unused heat (available for either heat recovery or cooling power). The combined overall efficiency of CCHP FCS (including electrical, heat, and cooling efficiency) can be greater than that of CHP FCSs when the LiBr ACC COP is greater than one.

References

[1] California Global Warming Solutions Act of 2006. Assembly Bill No. 32, State of California, Approved by the Governor and the Secretary of State September 27, 2006. Website: www.arb.ca.gov/cc/docs/ab32text.pdf.

[2] Executive Order S-3-05 by the Governor of the State of California, Executive Department, State of California, June 1, 2005. Website: www.dot.ca.gov/hq/energy/ExecOrderS-3-05.htm.

[3] W.G. Colella, S.H. Schneider, and D.M. Kammen, Mitigating Global Warming with Stationary Fuel Cell Systems (FCS): A Case Study of California, *Proceedings of the American Society of Mechanical Engineers (ASME) Second European Fuel Cell Technology & Applications Conference 2007*. New York, NY: American Society of Mechanical Engineers (ASME), 2007.

[4] W.G. Colella, S.H. Schneider, and D.M. Kammen, *Optimization of Novel Distributed Energy Networks to Reduce Greenhouse Gas Emissions in California,* (Stanford University and University of California, Berkeley). (California Energy Commission (CEC) Public Interest Energy Research (PIER) report), PIER Energy-Related Environmental Research Program, CEC-500-2008-030, 2008.

[5] C. Marnay and R. Firestone, Microgrids: An Emerging Paradigm for Meeting Building Electricity and Heat Requirements Efficiently and with Appropriate Energy Quality, *European Council for an Energy Efficient Economy 2007 Summer Study*. La Colle sur Lup, France, June 4-9, 2007.

[6] W.G. Colella, Implications of Electricity Liberalization for Combined Heat and Power (CHP) Fuel Cell Systems (FCSs): a Case Study of the United Kingdom, *Journal of Power Sources*, Vol. 106, pp. 397-404, April 2002.

[7] R. O'Hayre, S.W. Cha, W.G. Colella, and F.B. Prinz, *Fuel Cell Fundamentals*, 1st edition. John Wiley & Sons, Inc.: Hoboken, NJ, ISBN-13 978-0-471-74148-0 2006.

[8] R. O'Hayre, S.W. Cha, W.G. Colella, and F.B. Prinz, *Fuel Cell Fundamentals*, 2nd edition. John Wiley & Sons, Inc.: Hoboken, NJ, ISBN 978-0-470-25843-9, 2009.

[9] Environmental Protection Agency (EPA), *National Emissions Inventory*, 2002. Website: http://www.epa.gov/ttn/chief/net/2002inventory.html.

[10] W.G. Colella, (author) Chapter 45 in Schneider, S.H., Rosencranz, A. and Mastrandrea, M.D. (editors), Designing Energy Supply Chains Based on Hydrogen, *Climate Change Science and Policy, 2cd edition,* (Washington, D.C.: Island Press, 2010), pp. 456-466, 2010.

[11] W.G. Colella, S.H. Schneider, and D.M. Kammen, Mitigating Global Warming with Stationary Fuel Cell Systems (FCS): A Case Study of California, *Proceedings of the American Society of Mechanical Engineers (ASME) Second European Fuel Cell Technology & Applications Conference 2007*, (New York, NY: American Society of Mechanical Engineers (ASME), 2007.

[12] W.G. Colella, Optimal Design and Control Strategies for Novel Combined Heat and Power (CHP) Fuel Cell Systems: Part I of II – Datum Design Conditions and Approach, *Proceedings of the 8th International Fuel Cell Science, Engineering & Technology Conference*. New York, NY: American Society of Mechanical Engineers (ASME), ISBN 9780791838754, 2010.

[13] W.G. Colella, Optimal Design and Control Strategies for Novel Combined Heat and Power (CHP) Fuel Cell Systems: Part II of II – Case Study Results, *Proceedings of the 8th International Fuel Cell Science, Engineering & Technology Conference*, New York, NY: American Society of Mechanical Engineers (ASME), ISBN 9780791838754, 2010.

[14] W.G. Colella and A. Rankin, Network Design Optimization of Novel Fuel Cell Systems and Distributed Energy Devices: Model Development and Results, *Proceedings of European Fuel Cell Technology & Applications - "Piero Lunghi Conference."* Rome, Italy: American Society of Mechanical Engineers (ASME), ISBN 978-88-8286-211-4, 2009.

[15] W.G. Colella, Modeling Results for the Thermal Management Sub-System of a Combined Heat and Power (CHP) Fuel Cell System (FCS), *Journal of Power Sources*, Vol. 118, pp. 129-49, May 2003.

[16] W.G. Colella, Design Considerations for Effective Control of an Afterburner Sub-System in a Combined Heat and Power (CHP) Fuel Cell System (FCS), *Journal of Power Sources*, Vol. 118, pp. 118-28, May 2003.

[17] W.G. Colella, Design Options for Achieving a Rapidly Variable Heat-to-Power Ratio in a Combined Heat and Power (CHP) Fuel Cell System, *Journal of Power Sources*, Vol. 106, pp. 388-96, April 2002.

[18] W.G. Colella, C. Niemoth, C. Lim, and A. Hein, Evaluation of the Financial and Environmental Feasibility of a Network of Distributed 200 kWe Cogenerative Fuel Cell Systems on the Stanford University Campus, *Fuel Cells – From Fundamentals to Systems*, Vol. 1, pp. 148-166, February 2005.

[19] W.G. Colella, S.H. Schneider, D.M. Kammen, A. Jhunjhunwala, and N. Teo, Part I of II: Development of MERESS Model – Developing System Models Of Stationary Combined Heat And Power (CHP) Fuel Cell Systems (FCS) For Reduced Costs And Greenhouse Gas (GHG) Emissions, *Proceedings of the 6th International Fuel Cell Science, Engineering & Technology Conference*. New York, NY: American Society of Mechanical Engineers (ASME), ISBN 0-7918-3822-6, 2008.

[20] W.G. Colella, S.H. Schneider, D.M. Kammen, A. Jhunjhunwala, and N. Teo, Part II of II: Deployment of MERESS Model -- Designing, Controlling, And Installing Stationary Combined Heat And Power (CHP) Fuel Cell Systems (FCS) To Reduce Costs And Greenhouse Gas (GHG) Emissions, *Proceedings of the 6th International Fuel Cell Science, Engineering & Technology Conference*. New York, NY: American Society of Mechanical Engineers (ASME), ISBN 0-7918-3822-6, 2008.

[21] W.G. Colella S.H. Schneider, D.M. Kammen, A. Jhunjhunwala, and N. Teo, Optimizing the Design and Deployment of Stationary Combined Heat and Power (CHP) Fuel Cell Systems (FCS) for Minimum Costs and Emissions – Model Design (Part I of II), *ASME Journal of Fuel Cell Science and Technology*, 2010.

[22] W.G. Colella S.H. Schneider, D.M. Kammen, A. Jhunjhunwala, and N. Teo, Optimizing the Design and Deployment of Stationary Combined Heat and Power (CHP) Fuel Cell Systems (FCS) for Minimum Costs and Emissions – Model Results (Part II of II), *ASME Journal of Fuel Cell Science and Technology*, 2010.

[23] W.G. Colella, A. Rankin, A. Sun, P. Margalef, and J. Brouwer, Thermodynamic, Economic, and Environmental Modeling of Hydrogen (H_2) Co-Production Integrated with Stationary Fuel Cell Systems (FCS), poster presentation, *2009 U.S. Department of Energy Hydrogen Program Annual Merit Review & Peer Evaluation Meeting*. Arlington, VA, May 18-22, 2009.

[24] P. Margalef, *The Integration of a High Temperature Fuel Cell and Absorption Chiller into a Generic Building*, Master's Thesis Report, University of California, Irvine, 2007.

[25] W.G. Colella and A., Rankin, Designing Combined Cooling, Heating, and Electric Power (CCHP) Fuel Cell Systems, *Proceedings of European Fuel Cell Technology & Applications - "Piero Lunghi Conference*. Rome, Italy: American Society of Mechanical Engineers (ASME), ISBN 978-88-8286-211-4, 2009.

[26] W.G. Colella, Designing Combined Cooling, Heating, And Electric Power (CCHP) Fuel Cell Systems (FCS), *Proceedings of the 8th International Fuel Cell Science, Engineering & Technology Conference*. New York, NY: American Society of Mechanical Engineers (ASME), ISBN 9780791838754, 2010.

[27] W.G. Colella, J. Brouwer, S. Kelly, P. Margalef, and M. Parker, Thermodynamic and Chemical Engineering Models of Combined Cooling, Heating, and Electric Power (CCHP) Fuel Cell Systems, *Proceedings of European Fuel Cell Technology & Applications - "Piero Lunghi Conference."* Rome, Italy: American Society of Mechanical Engineers (ASME), ISBN 978-88-8286-211-4, 2009.

[28] H. Ghezel-Ayagh, A.J. Leo, H. Maru, and M. Farooque, Overview of Direct Carbonate Fuel Cell Technology and Products Development, *ASME First International Conference on Fuel Cell Science, Energy and Technology*, Rochester, NY, p. 11, April 21-23, 2003.

[29] Stanford Electricity, Cooling and Heating Demand Data 2007. *Real-Time Electricity, Cooling and Heating Demand Data for Stanford University Campus Buildings, 2007*; Facilities Operations – Utilities Department, Stanford University, 327 Bonair Siding, Stanford, California, 94305-7272.

[30] R. Huisman, C. Huurman, and R. Mahieu, *Hourly Electricity Prices in Day-Ahead Markets.* Erasmus Research Institute Report, Erasmus Research Institute of Management Research

In Management Report Series, Erasmus University, The Netherlands, 2007.

[31] B. Shaffer, and J. Brouwer, Quasi-3-D dynamic model of an internally reforming planar solid oxide fuel cell for hydrogen co-production, *Proceedings of FuelCell2008 Sixth International Fuel Cell Science, Engineering and Technology Conference,* Denver, CO, June 16-18, 2008.

[32] *2009 ASHRAE Handbook - Fundamentals*. American Society of Heating, Refrigerating and Air-Conditioning Engineers, Inc., 2009.

[33] B. Shaffer, M. Hunsuck, and J. Brouwer, Quasi-3-D dynamic model of an internally reforming planar solid oxide fuel cell for hydrogen co-production, *Proceedings of FuelCell2008 Sixth International Fuel Cell Science, Engineering and Technology Conference,* Denver, CO, June 16-18, 2008.

[34] G. Vliet, M. B. Lawson, and R.A. Lithgow, *Water-lithium bromide double effect absorption cooling analysis*, Center for Energy Studies of the University of Texas at Austin, 1980.

[35] Yazaki Energy, *Dual Fired Chiller-Heater KE Model. 1 Specifications*, 2003.

[36] G.M. Whitesides and G. W. Crabtree, Don't Forget Long-Term Fundamental Research in Energy, *Science*, Vol. 315, No. 5813, pp. 796 – 798, February 9, 2007.

DISTRIBUTION

2	MS 0899	Technical Library	9536 *(1 electronic and 1 paper copy)*